Inorganic Chemistry

Article

pubs.acs.org/IC

Revelation of Varying Coordination Modes and Noninnocence of Deprotonated 2,2′-Bipyridine-3,3′-diol in {Os(bpy)$_2$} Frameworks

Prabir Ghosh, Ritwika Ray, Ankita Das, and Goutam Kumar Lahiri*

Department of Chemistry, Indian Institute of Technology Bombay, Powai, Mumbai 400076, India

Supporting Information

ABSTRACT: The reaction of 2,2′-bipyridine-3,3′-diol (H_2L) and *cis*-$Os^{II}(bpy)_2Cl_2$ (bpy = 2,2′-bipyridine) results in isomeric forms of $[Os^{II}(bpy)_2(HL^-)]ClO_4$, $[\mathbf{1}]ClO_4$ and $[\mathbf{2}]ClO_4$, because of the varying binding modes of partially deprotonated HL^-. The identities of isomeric $[\mathbf{1}]ClO_4$ and $[\mathbf{2}]ClO_4$ have been authenticated by their single crystal X-ray structures. The ambidentate HL^- in $[\mathbf{2}]ClO_4$ develops the usual N,N bonded five-membered chelate with a strong O−H···O hydrogen bonded situation (O−H···O angle: 160.78°) at its back face. The isomer $[\mathbf{1}]ClO_4$ however represents the monoanionic O^-,N coordinating mode of HL^-, leading to a six-membered chelate with the moderately strong O−H···N hydrogen bonding interaction (O−H···N angle: 148.87°) at its backbone. The isomeric $[\mathbf{1}]ClO_4$ and $[\mathbf{2}]ClO_4$ also exhibit distinctive spectral, electrochemical, electronic structural, and hydrogen bonding features. The pK_a values for $[\mathbf{1}]ClO_4$ and $[\mathbf{2}]ClO_4$ have been estimated to be 0.73 and <0.2, respectively, thereby revealing the varying hydrogen bonding interaction profiles of O−H···N and O−H···O involving the coordinated HL^-. The O−H···O group of HL^- in $\mathbf{2}^+$ remains invariant in the basic region (pH 7−12), while deprotonation of O−H···N group of HL^- in $\mathbf{1}^+$ estimates the pK_b value of 11.55. This indeed has facilitated the activation of the exposed O−H···N function in $[\mathbf{1}]ClO_4$ by the second $\{Os^{II}(bpy)_2\}$ unit to yield the L^{2-} bridged $[(bpy)_2Os^{II}(\mu\text{-}L^{2-})Os^{II}(bpy)_2](ClO_4)_2$ ($[\mathbf{3}](ClO_4)_2$). However, the O−H···O function in $[\mathbf{2}]ClO_4$ fails to react with $\{Os^{II}(bpy)_2\}$. The crystal structure of $[\mathbf{3}](ClO_4)_2$ establishes the symmetric N,O^-/O^-,N bridging mode of L^{2-}. On the other hand, the doubly deprotonated L'^{2-} (H_2L' = 2,2′-biphenol) generates structurally characterized twisted seven-membered O^-,O^- bonded chelate (torsion angle >50°) in paramagnetic $[Os^{III}(bpy)_2(L'^{2-})]ClO_4$ ($[\mathbf{4}]ClO_4$). The electronic structural aspects of the complexes reveal the noninnocent potential of the coordinated HL^-, L^{2-}, and L'^{2-}. The K_c value of 49 for $\mathbf{3}^{3+}$ reveals a class I mixed-valent $Os^{II}Os^{III}$ state.

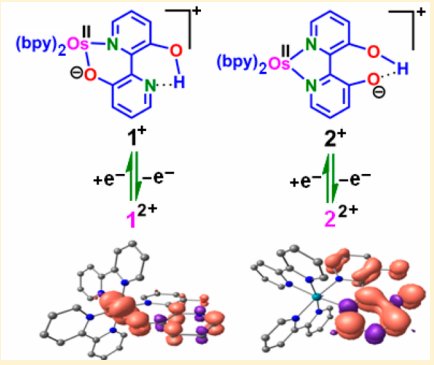

INTRODUCTION

The pH dependent proton-shuttling process involving a pendant OH or NH group of a metal coordinated ligand is known to facilitate catalytic processes by releasing or accepting the proton, leading to a tunable electronic situation around the metal ions.[1] It is therefore imperative to design newer molecular frameworks with integrated pH sensitive functionalities. In this regard, the ambidentate ligand 2,2′-bipyridine-3,3′-diol (H_2L) incorporating suitably positioned nitrogen donors as well as dissociable hydroxyl protons has the potential to develop metal complexes with accessible OH groups or hydrogen bonded O−H···O/O−H···N functionalities at its back face. The built in rotational flexibility of the two rings of H_2L with respect to the connecting C−C single bond and pH driven deprotonation process may lead to its multiple coordinating modes: (a) N,N donating H_2L with free OH groups, (b) N,N donating HL^- with O−H···O function, (c) N,O^- donating HL^- with O−H···N function, (d) O^-,O^- donating L^{2-}, as well as (e) symmetric (N,O^-/O^-,N) and (f) asymmetric (N,N/O^-O^-) bridging modes of L^{2-} (Scheme 1).

The coordinating modes **a** and **b** (Scheme 1) are reported in transition metal complexes of Re(I)/Ru(II)[2] and Ru(II),[3] Cu(II),[4a−c] Co(III),[4c,d] Ir(III),[5] Pd(II),[6] Zn(II),[7] and Cd(II),[8] respectively. The unusual O^-,O^- bonded situation of deprotonated L^{2-} leading to a twisted seven-membered chelate (**d**, Scheme 1) has been established recently, selectively with $\{Ru^{II}(pap)_2\}$ metal fragment incorporating strongly π-acidic pap[9] (pap = 2-phenylazopryridine) coligand.[3b] The symmetric

Scheme 1. Probable Coordination Modes of H_2L and Its Deprotonated Forms

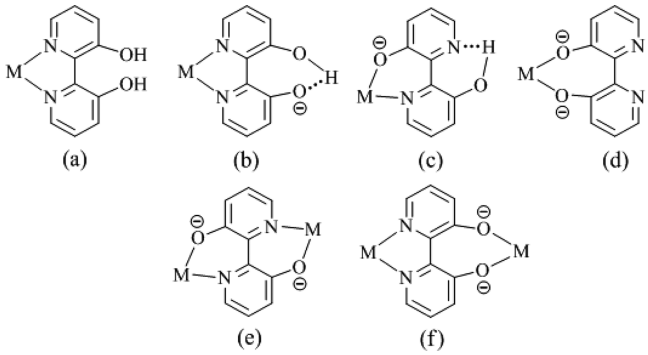

Received: July 30, 2014
Published: September 23, 2014

Scheme 2. Schematic Representation of Reaction Profiles

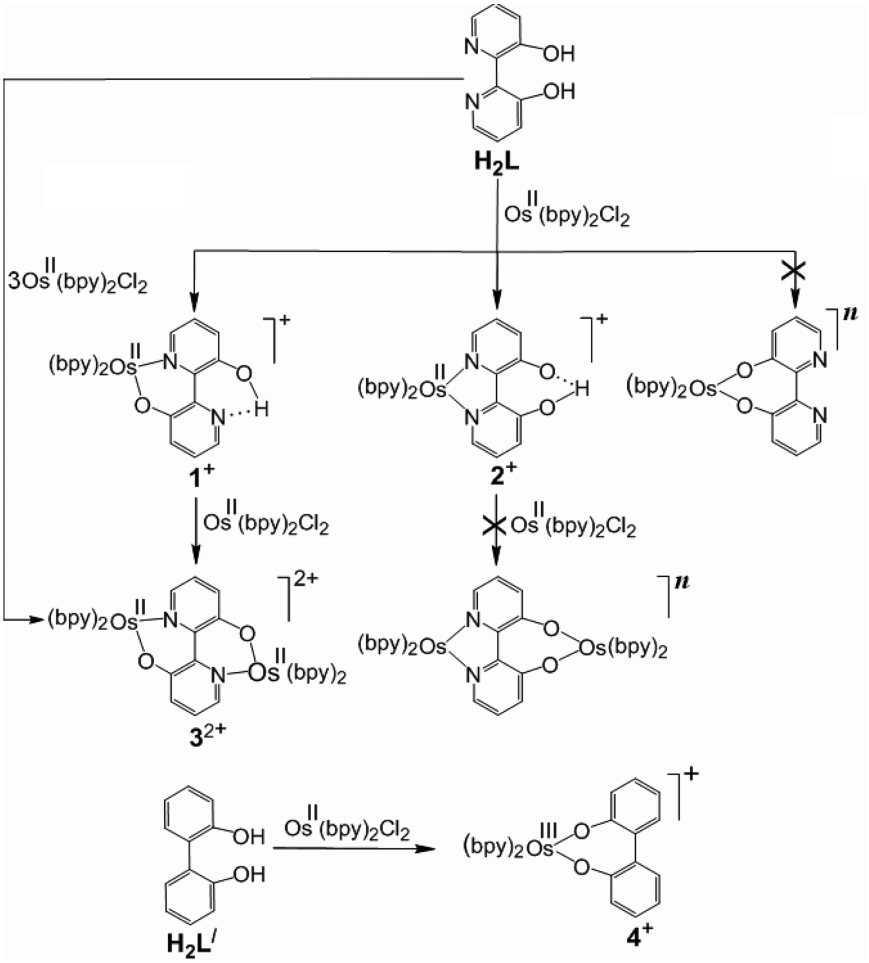

bridging mode of L^{2-} (**e**, Scheme 1) has also been described in $[(bpy)_2Ru^{II}(\mu\text{-}L^{2-})Ru^{II}(bpy)_2](PF_6)_2$ (bpy = 2,2′-bipyridine)[3a] and $[(pap)_2Ru^{II}(\mu\text{-}L^{2-})Ru^{II}(pap)_2](ClO_4)_2$.[3b] However, to the best of our knowledge, the other probable coordinating modes, i.e. N,O^- bonded HL^- with O−H···N hydrogen bonding interaction at its back face (**c**) and asymmetric N,N/O^-,O^- bridging mode of L^{2-} (**f**, Scheme 1) have not been recognized so far.

This indeed has been the genesis of the present work of exploring the viability of stabilizing the missing coordinating modes, **c** and/or **f** (Scheme 1) involving partially and fully deprotonated H_2L, respectively, by introducing suitable metal fragments. This has however been achieved via selective introduction of the $\{Os^{II}(bpy)_2\}$ metal fragment, leading to the formation of isomeric forms of $[Os^{II}(bpy)_2(HL^-)]^+$, $\mathbf{1}^+$ and $\mathbf{2}^+$, where the former represents the hitherto unrecognized N,O^- coordinating mode of HL^- (**c**, Scheme 1) and the latter comprises the usual N,N donating mode of HL^- (**b**, Scheme 1). Importantly, isomeric $\mathbf{1}^+$ and $\mathbf{2}^+$ extend the unique feature of varying hydrogen bonding patterns, O−H···N and O−H···O, respectively, involving the coordinated HL^-.

The present article highlights the structural, spectral, and electrochemical aspects as well as pH driven processes of isomeric $[\mathbf{1}]ClO_4$ and $[\mathbf{2}]ClO_4$. It also discusses the structural and spectro-electrochemical features of the deprotonated L^{2-} bridged symmetric $[(bpy)_2Os^{II}(\mu\text{-}L^{2-})Os^{II}(bpy)_2](ClO_4)_2$, $[\mathbf{3}](ClO_4)_2$ (**e**, Scheme 1) and paramagnetic $[Os^{III}(bpy)_2(L'^{2-})]ClO_4$, $[\mathbf{4}]ClO_4$, involving relatively less known sterically constrained seven-membered chelate situation with L'^{2-} (H_2L' = 2,2′-biphenol) (Scheme 2). Moreover, electronic structural aspects of the complexes including noninnocent potential of the coordinated HL^-, L^{2-}, and L'^{2-} have been evaluated by experimental and DFT calculations.

It should be noted that the present work demonstrates the first set of osmium complexes involving H_2L or its deprotonated form. Interestingly, the analogous ruthenium derivatives of H_2L/HL^- are reported to exhibit excellent cytotoxicity toward A2780 human ovarian and 549 human lung cancer cells.[2b]

RESULTS AND DISCUSSION

Synthesis and Characterization. The isomeric $\mathbf{1}^+$ (red) and $\mathbf{2}^+$ (yellow) of the molecular composition of $[Os^{II}(bpy)_2(HL^-)]^+$ (Scheme 2) have been obtained in almost 1:1 ratio from $Os^{II}(bpy)_2Cl_2$ (bpy = 2,2′-bipyridine) and H_2L (H_2L = 2,2′-bipyridine-3,3′-diol) in the presence of NEt_3 as a base in refluxing ethanol−water (1:1) followed by chromatographic separation on a neutral alumina column (see Experimental Section). Crystal structures of the isolated $[\mathbf{1}]ClO_4$ and $[\mathbf{2}]ClO_4$ (see later) reveal that the isomers differ with respect to the conceivable varying binding modes of the coordinated monodeprotonated HL^-. Though HL^- in $\mathbf{2}^+$ demonstrates its usual N,N-coordinating mode with a strong intramolecular O−H···O hydrogen bonding interaction at its back face (**b**, Scheme

dx.doi.org/10.1021/ic501852a | Inorg. Chem. 2014, 53, 10695−10707

1), isomer $\mathbf{1}^+$ represents the mixed O^-,N donating feature of HL^- involving a moderately strong O–H···N hydrogen bonding situation at its exposed outer face (**c**, Scheme 1). The other probable O^-,O^--coordinating mode of the fully deprotonated L^{2-} leading to a seven-membered chelate (**d**, Scheme 1) has not been realized with the $\{Os^{II}(bpy)_2\}$ metal fragment. However, the same O^-,O^--bonded L^{2-} has recently been reported, selectively with $\{Ru^{II}(pap)_2\}$ metal fragment incorporating strongly π-acidic pap (pap = 2-phenylazopyridine).[3b] The stronger π-donor or weaker π-acceptor feature of $\{Os^{II}(bpy)_2\}$ as compared to $\{Ru^{II}(pap)_2\}$[10] hinders the formation of a sterically constrained seven-membered chelate situation involving O^-,O^--bonded L^{2-}; instead, it stabilizes the theromodynamically favored six (O^-,N donors) and five-membered (N,N donors) chelates[11] in $\mathbf{1}^+$ and $\mathbf{2}^+$, respectively. However, the deprotonated L'^{2-} (H_2L' = 2,2′-biphenol) easily develops the less common[12] and twisted seven-membered chelate in paramagnetic $[Os^{III}(bpy)_2(L'^{2-})]^+$ ($\mathbf{4}^+$, Scheme 2) via the available O^-,O^- donors. This essentially implies that under an optional condition as in the case of H_2L [O^-,O^- donors (seven-membered) or O^-,N donors (six-membered) or N,N donors (five-membered)] $\{Os^{II}(bpy)_2\}$ prefers the six- as well as five-membered chelate situations of HL^- in $\mathbf{1}^+$ and $\mathbf{2}^+$, respectively, over the constrained O^-,O^- bonded seven-membered chelate involving L^{2-}. It is noteworthy that, unlike the reported $[Ru^{II}(bpy)_2(L'^{2-})]$[13] and $[Ru^{II}(pap)_2(L'^{2-})]$,[3b] the doubly deprotonated L'^{2-} stabilizes osmium ion in one-electron paramagnetic +3 oxidation state (t_{2g}^5) in $[\mathbf{4}]ClO_4$ (μ = 1.82 μ_B),[14] due to the better π-donor feature of $\{Os^{II}(bpy)_2\}$.

All attempts to activate the available O–H···O hydrogen bond associated with the coordinated HL^- in $\mathbf{2}^+$ by another molecule of $\{Os^{II}(bpy)_2\}$ have failed which indeed has restricted us to obtain the unrecognized asymmetric L^{2-} bridged (N,N and O^-,O^-) dimeric species (**f**, Scheme 1). However, facile activation of the exposed O–H···N hydrogen bond of HL^- in $\mathbf{1}^+$ by another $\{Os^{II}(bpy)_2\}$ unit results in symmetric L^{2-} bridged (O^-,N and N,O^-) dimeric species $[(bpy)_2Os^{II}(\mu\text{-}L^{2-})Os^{II}(bpy)_2]^{2+}$ (**e**, Schemes 1 and $\mathbf{3}^{2+}$, Scheme 2). The dimeric $\mathbf{3}^{2+}$ has also been prepared directly from a 3:1 mixture of $Os^{II}(bpy)_2Cl_2$ and H_2L in refluxing ethanol–water (1:1) and in the presence of NEt_3 as a base, but it gives much lesser yield as compared to that obtained via the reaction of $\mathbf{1}^+$ and $Os^{II}(bpy)_2Cl_2$ in 1:1 ratio (Scheme 2, Experimental Section).

The complexes $[\mathbf{1}]ClO_4$, $[\mathbf{2}]ClO_4$, $[\mathbf{3}](ClO_4)_2$, and $[\mathbf{4}]ClO_4$ exhibit expected electrical conductivities, $\nu(ClO_4)$ vibrations in their IR spectra, and satisfactory microanalytical data (Experimental Section). The identities of the complexes in the solution state have been established by mass spectrometry whichs show molecular ion peaks at 691.1357, 691.1357, 596.1450, and 688.1291 corresponding to $\mathbf{1}^+$ (calculated mass: 691.1415), $\mathbf{2}^+$ (calculated mass: 691.1415), $\{[\mathbf{3}]^{2+}/2\}$ (calculated mass: 596.1169), and $\mathbf{4}^+$ (calculated mass: 688.1472), respectively (Figure S1, Supporting Information and Experimental Section).

Molecular Structures. Molecular structures of all the four complexes ($[\mathbf{1}]ClO_4$, $[\mathbf{2}]ClO_4$, $[\mathbf{3}](ClO_4)_2$, $[\mathbf{4}]ClO_4$) have been authenticated by their single crystal X-ray structures (Figures 1–4). The selected crystallographic parameters and bond lengths are set in Table 1 and Tables 2 and 3, respectively. The selected bond angles are listed in Tables S1 and S2, Supporting Information. The experimental bond parameters are matching well with the DFT calculated values

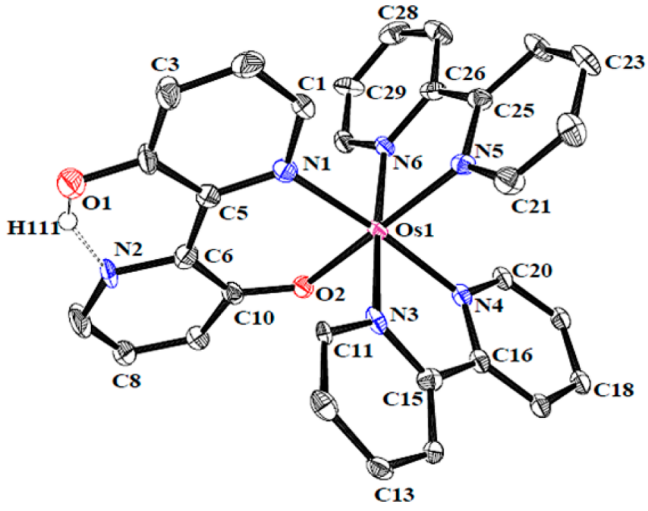

Figure 1. ORTEP diagram of the cation of $[\mathbf{1}]ClO_4$. Ellipsoids are drawn at 50% probability level. Hydrogen atoms are omitted for clarity.

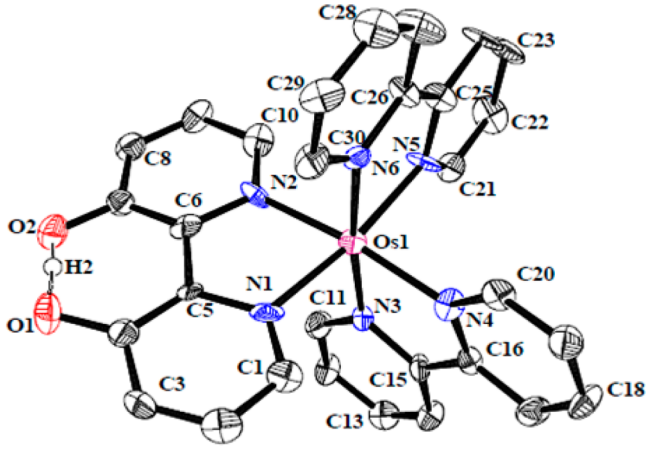

Figure 2. ORTEP diagram of the cation of $[\mathbf{2}]ClO_4$. Ellipsoids are drawn at 50% probability level. Hydrogen atoms are omitted for clarity.

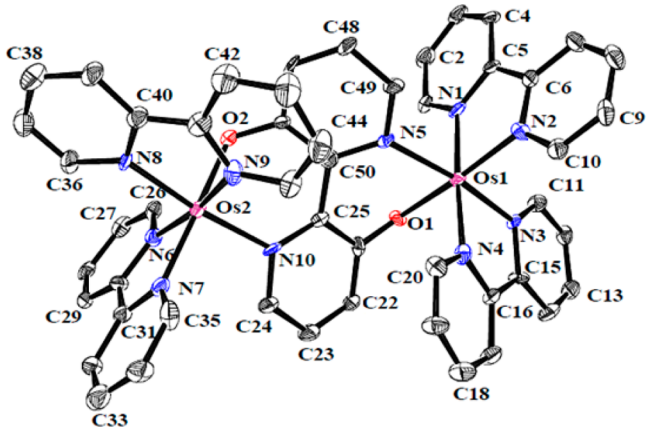

Figure 3. ORTEP diagram of the cation of $[\mathbf{3}](ClO_4)_2$. Ellipsoids are drawn at 50% probability level. Hydrogen atoms and solvent molecules are omitted for clarity.

(Tables 2 and 3 and Tables S1 and S2, Supporting Information). Crystal structures establish that the monodeprotonated HL^- in isomeric $\mathbf{1}^+$ and $\mathbf{2}^+$ is bonded through the

dx.doi.org/10.1021/ic501852a | Inorg. Chem. 2014, 53, 10695–10707

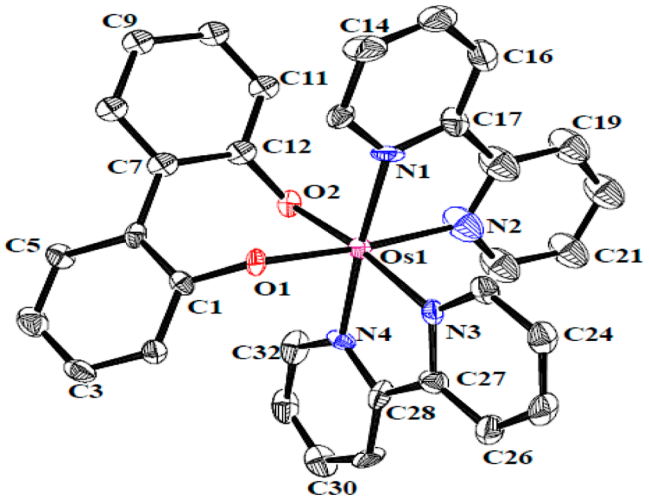

Figure 4. ORTEP diagram of the cation of one of the molecules (molecule A) in the asymmetric unit of [**4**]ClO_4. Ellipsoids are drawn at 50% probability level. Hydrogen atoms and solvent molecule are omitted for clarity.

mixed N,O^- and N,N donors, leading to six- and five-membered chelates, respectively. It also reveals the existence of O—H···N and O—H···O hydrogen bonding interactions at the backbone of the coordinated HL^- in $\mathbf{1}^+$ and $\mathbf{2}^+$, respectively. The angles associated with O—H···N in $\mathbf{1}^+$ (148.87°) and O—H···O in $\mathbf{2}^+$ (160.78°) imply moderately strong and negative charge assisted strong hydrogen bonding interactions, respectively.[15] Consequently, the nonbonded O1—N2 distance involving O1—H···N2 in $\mathbf{1}^+$ of 2.425 Å is longer than O1—O2 distance of 2.386 Å for O1—H···O2 in $\mathbf{2}^+$. The bond angles around the osmium centers suggest distorted octahedral arrangements in $\mathbf{1}^+$ and $\mathbf{2}^+$. The bite angle involving six-membered chelate of HL^- in $\mathbf{1}^+$ of 90.14(14)° is expectedly much larger than that associated with the five-membered chelate of HL^- in $\mathbf{2}^+$ of 77.5(4)°. The near planar feature of HL^- in $\mathbf{1}^+$ and $\mathbf{2}^+$ has been validated by the torsion angles involving N1—C5—C6—C10 and N1—C5—C6—N2 of 0.3(8)° and 8.4(12)°, respectively. The ring connecting C5—C6 single bond distances of 1.485(6) and 1.503(15) Å in $\mathbf{1}^+$ and $\mathbf{2}^+$, respectively, match well with that of analogous ruthenium derivative $Ru^{III}(acac)_2(HL^-)$ (1.475(3) Å) incorporating N,N coordinating HL^- (acac = acetylacetonate)[3b] which in fact rules out the alternate tautomeric forms $\mathbf{1a}^+$ and $\mathbf{2a}^+$ (Scheme 3).[3a] This has further been supported by the single bond lengths of C4—O1/C10—O2, 1.324(6) Å/1.288(6) Å and C4—O1/C7—O2, 1.329(14) Å/1.320(14) Å involving HL^- in $\mathbf{1}^+$ and $\mathbf{2}^+$, respectively. The average Os^{II}—N(bpy) bond lengths, 2.049(4) Å and 2.073(9) Å in $\mathbf{1}^+$ and $\mathbf{2}^+$, respectively, are in agreement with that reported for $[Os^{II}(bpy)_3]^{2+}$ (2.056(8) Å).[16] The Os^{II}—O^- (phenolato) bond length of 2.067(3) Å in $\mathbf{1}^+$ matches closely to that reported for $[Os^{II}(bpy)_2(O—C_7H_6)N{=}N—C_7H_7)]^+$ (2.078(5) Å).[17] The Os^{II}—N(HL^-) distance in $\mathbf{1}^+$ (2.102(4) Å) is appreciably longer than that in $\mathbf{2}^+$ (average, 2.066(10) Å).

The crystal structure of $\mathbf{3}^{2+}$ establishes that the doubly deprotonated L^{2-} bridges the two $\{Os^{II}(bpy)_2\}$ units symmetrically via its mixed N,O^- donor sets, leading to a six-membered chelate at each end. The OsN_5O chromophore in $\mathbf{3}^{2+}$ exhibits distorted octahedral geometry as in mononuclear $\mathbf{1}^+$. However, unlike HL^- in $\mathbf{1}^+$, the two rings of bridging L^{2-} in $\mathbf{3}^{2+}$ are appreciably twisted with the torsion angles, N10−C25−C50−C46 and N5−C50−C25−C21 of 36.18(4)° and 36.83(7)°, respectively, similar to that reported for $[\{Ru^{II}(pap)_2\}_2(\mu\text{-}L^{2-})](ClO_4)_2$ (37.33°/38.33°).[3b] However, the nonplanarity of L^{2-} in $\mathbf{3}^{2+}$ is much lesser than that of L'^{2-} in $\mathbf{4}^+$ (torsion angle >50°, see below). The Os^{II}—N(L^{2-}) bond lengths (Os1−N5, 2.108(6) Å; Os2−N10, 2.090(6) Å) are longer than Os^{II}—O^-(L^{2-}) bond lengths (Os1−O1, 2.076(5) Å Os2−O2, 2.074(5) Å) in $\mathbf{3}^{2+}$ as in $\mathbf{1}^+$. The single bond lengths of ring connecting C25−C50 (1.481(10) Å) and

Table 1. Selected Crystallographic Parameters for [1]ClO_4, [2]ClO_4, [3]$(ClO_4)_2$·C_7H_8·CH_2Cl_2·$2H_2O$, and 2[4]ClO_4·$CHCl_3$

	[**1**]ClO_4	[**2**]ClO_4	[**3**]$(ClO_4)_2$·C_7H_8·CH_2Cl_2·H_2O	2[**4**]ClO_4·$CHCl_3$
empirical formula	$C_{30}H_{23}ClN_6O_6Os$	$C_{30}H_{23}ClN_6O_8Os$	$C_{58}H_{40}Cl_4N_{10}O_{11}Os_2$	$C_{65}H_{49}Cl_5N_8O_{12}Os_2$
fw	789.19	789.19	158.26	1691.77
cryst syst	triclinic	triclinic	monoclinic	triclinic
space group	$P\bar{1}$	$P\bar{1}$	$P2_1/c$	$P\bar{1}$
a (Å)	8.608(2)	8.899(11)	20.194(3)	12.791 (5)
b (Å)	13.845(4)	11.948(14)	20.023 (3)	12.816 (5)
c (Å)	14.172(4)	15.427(19)	14.143 (2)	20.033 (7)
α (deg)	77.118(10)	96.098(15)	90	98.293 (3)
β (deg)	72.478(10)	105.56(3)	96.572 (2)	98.983 (4)
γ (deg)	84.891(13)	93.292(19)	90	107.565 (3)
V (Å^3)	1569.6(7)	1565(3)	5681.1 (14)	3028 (2)
Z	2	2	4	2
μ (mm^{-1})	4.198	4.211	4.73	4.486
T (K)	100(2)	100(2)	100(2)	100(2)
D_{calcd} (g cm^{-3})	1.670	1.675	1.851	1.856
F(000)	772	772	3096	1656
θ range (deg)	3.02−25.00	3.06−25.00	3.05−29.23	3.03−25.0
data/restraints/params	5495/62/397	5508/7/398	15 372/58/754	10 349/219/809
R1, wR2 [$I > 2\sigma(I)$]	0.0332, 0.0669	0.0658, 0.1749	0.0642, 0.1674	0.0672, 0.1661
R1, wR2 (all data)	0.0384, 0.0697	0.0749, 0.1858	0.0777, 0.1801	0.0765, 0.1816
GOF	1.005	1.089	1.110	0.979
largest diff peak/hole, (e Å^{-3})	1.380 and −1.018	2.341 and −2.680	4.70 and −2.42	3.32 and −1.90

dx.doi.org/10.1021/ic501852a | Inorg. Chem. 2014, 53, 10695−10707

Table 2. Experimental and DFT Calculated Selected Bond Lengths (Å) for $[1]ClO_4$ and $[2]ClO_4$

$[1]ClO_4$			$[2]ClO_4$		
bond length (Å)	X-ray	DFT	bond length (Å)	X-ray	DFT
Os1−N1	2.102(4)	2.152	Os1−N1	2.086(10)	2.091
Os1−O2	2.067(3)	2.063	Os1−N2	2.047(10)	2.092
Os1−N3	2.059(4)	2.072	Os1−N3	2.071(9)	2.085
Os1−N4	2.053(4)	2.068	Os1−N4	2.068(9)	2.095
Os1−N5	2.038(4)	2.075	Os1−N5	2.090(9)	2.096
Os1−N6	2.044(4)	2.075	Os1−N6	2.064(9)	2.086
C4−O1	1.324(6)	1.329	C4−O1	1.329(14)	1.280
C10−O2	1.288(6)	1.312	C7−O2	1.320(14)	1.300
C5−C6	1.485(6)	1.484	C5−C6	1.503(15)	1.476
O1−H111	0.84	1.017	O2−H2	0.840	1.300
N2···H111	1.668	1.577	O1···H2	1.577	1.099
O1···N2	2.425	2.506	O1···O2	2.386	2.395

Table 3. Experimental and DFT Calculated Selected Bond Lengths (Å) for $[3](ClO_4)_2{\cdot}C_7H_8{\cdot}CH_2Cl_2{\cdot}H_2O$ and $[4]ClO_4{\cdot}CHCl_3$

$[3](ClO_4)_2\ C_7H_8{\cdot}CH_2Cl_2{\cdot}H_2O$			molecule A $2[4]ClO_4{\cdot}CHCl_3$			molecule B $2[4]ClO_4{\cdot}CHCl_3$	
bond length (Å)	X-ray	DFT	bond length (Å)	X-ray	DFT	bond length (Å)	X-ray
Os1−N1	2.038(6)	2.078	Os1−N1	2.056(9)	2.078	Os2−N5	2.061(9)
Os1−N2	2.032(6)	2.072	Os1−N2	2.037(11)	2.117	Os2−N6	2.055(10)
Os1−N3	2.025(5)	2.066	Os1−N3	2.068(9)	2.118	Os2−N7	2.067(9)
Os1−N4	2.050(6)	2.069	Os1−N4	2.057(9)	2.078	Os2−N8	2.047(9)
Os1−N5	2.108(6)	2.170	Os1−O1	2.008(7)	1.997	Os2−O3	2.002(8)
Os1−O1	2.076(5)	2.070	Os1−O2	2.018(7)	1.997	Os2−O4	2.003(7)
Os2−N6	2.049(6)	2.078	C1−O1	1.389 (13)	1.361	C33−O3	1.356 (13)
Os2−N7	2.025(6)	2.071	C12−O2	1.355(14)	1.361	C44−O4	1.387 (14)
Os2−N8	2.039(6)	2.067	C6−C7	1.471 (16)	1.491	C38−C39	1.502 (18)
Os2−N9	2.040(6)	2.069					
Os2−N10	2.090(6)	2.170					
Os2−O2	2.074(5)	2.070					
C21−O1	1.331(8)	1.313					
C46−O2	1.330(8)	1.312					
C25−C50	1.481(10)	1.491					
Os1···Os2	6.253	6.409					
Os2−N9	2.040(6)	2.069					
Os2−N10	2.090(6)	2.170					

Scheme 3. Tautomeric Forms of $1^+/1a^+$ and $2^+/2a^+$

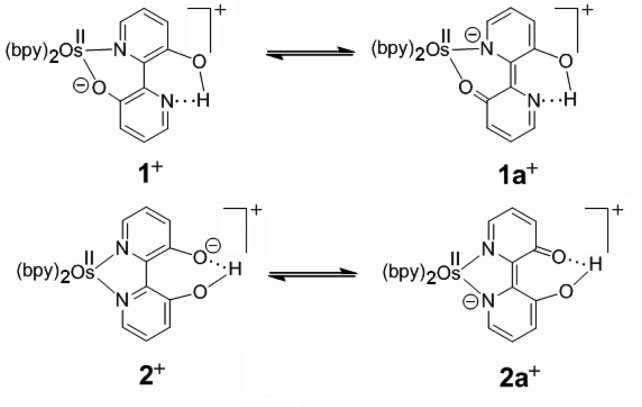

Scheme 4. Tautomeric Form of $3^{2+}/3a^{2+}$

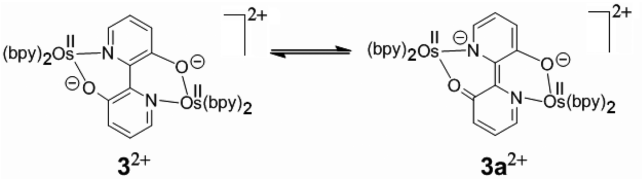

C21−O1/C46−O2 (1.331(8) Å/1.330(8) Å) of L^{2-} in 3^{2+} discard the tautomeric form $3a^{2+}$ (Scheme 4).[3a]

The crystal structure of $[Os^{III}(bpy)_2(L'^{2-})]ClO_4$ ($[4]ClO_4$) divulges the presence of two independent molecules (Figure S2, Supporting Information) in the asymmetric unit with slight differences in bond parameters, possibly due to crystal packing forces.[18] The nonplanarity of the seven-membered chelate involving doubly deprotonated L'^{2-} in the two molecules of 4^+ has been reflected in the torsion angles, C1−C6−C7−C12 and C33−C38−C39−C44 of 57.72(7)° and 50.13(5)°, respectively. The torsion angles of 4^+ are close to that reported for the analogous ruthenium complexes, $[Ru^{II}(bpy)_2(L'^{2-})]$ (58.5°)[13] and $[Ru^{II}(pap)_2(L'^{-})]$ (51.5°).[3b] The average *cis* (82.38(4)°) and *trans* (172.516(3)°) angles around the osmium ion in 4^+ are suggestive of a distorted octahedral situation. The average Os^{III}−N(bpy) and Os^{III}−$O^-(L'^{2-})$ bond lengths in 4^+ of 2.056(9) and 2.007(13) Å, respectively, are similar to those of reported analogous osmium(III) complexes, $[Os^{III}(bpy)_3](PF_6)_3$ (2.079(6) Å)[19] and $PPh_4[Os^{III}\{N(H)C(NH_2)_2\}(CN)_3(C_{13}H_8ONO^-)]$ (2.043(2) Å).[20] The single bond

dx.doi.org/10.1021/ic501852a | Inorg. Chem. 2014, 53, 10695−10707

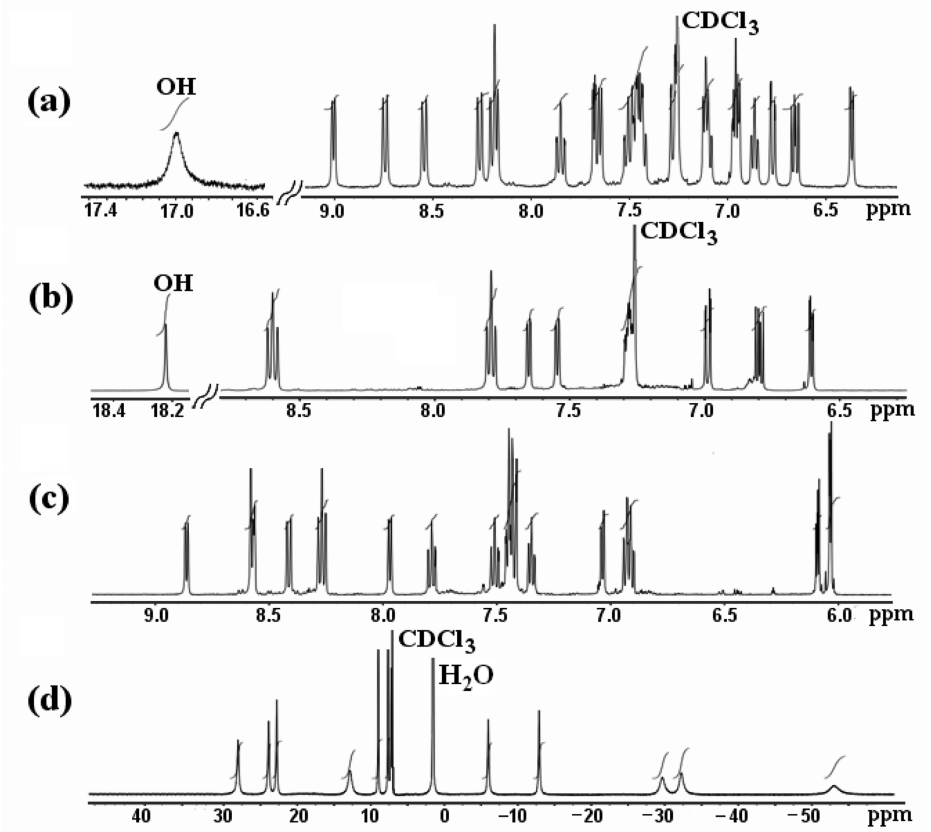

Figure 5. ^{1}H NMR spectra of (a) [**1**]ClO_4 (in $CDCl_3$), (b) [**2**]ClO_4 (in $CDCl_3$), (c) [**3**]$(ClO_4)_2$ (in CD_3CN), and (d) [**4**]ClO_4 (in $CDCl_3$).

lengths of C1−O1, C12−O2, and C6−C7 (ring connecting)/C33−O3, C44−O4, and C38−C39 (ring connecting) involving L'^{2-} in the two molecules of $\mathbf{4}^+$ are 1.389(13) Å, 1.355(14) Å and 1.471(16) Å/1.356(13) Å, 1.387(14) Å and 1.502(18) Å, respectively.

Spectral Aspects. ^{1}H NMR spectra of the complexes in different deuterated solvents are shown in Figure 5, and the data sets are in the Experimental Section. The diamagnetic isomeric complexes $\mathbf{1}^+$ and $\mathbf{2}^+$ are quite distinctive with respect to their NMR spectral profiles. $\mathbf{1}^+$ and $\mathbf{2}^+$ exhibit partially overlapping calculated number of 22 and 11 aromatic protons of bpy and HL^- in the chemical shift region δ 9.0−6.0 ppm corresponding to the full molecule and half molecule due to internal mirror symmetry, respectively. The O−H···N and O−H···O hydrogen bonded protons in $\mathbf{1}^+$ and $\mathbf{2}^+$ appear at δ 17 and 18.2 ppm, respectively. The stronger O−H···O hydrogen bonding interaction in $\mathbf{2}^+$ has been reflected in the appreciably downfield shifted OH proton resonance in $\mathbf{2}^+$ as compared to that associated with the O−H···N in $\mathbf{1}^+$.[15e,f,21] This has also been evidenced in the crystal structure parameters of $\mathbf{1}^+$ and $\mathbf{2}^+$ (see above). The L^{2-} bridged symmetric diosmium complex $\mathbf{3}^{2+}$ exhibits 19 partially overlapping aromatic proton resonances of bpy and L^{2-} over the chemical shift range δ 9.0−6.0 ppm corresponding to the half molecule due to the effect of internal inversion center. The paramagnetic feature of $[Os^{III}(bpy)_2(L'^{2-})]^+$ ($\mathbf{4}^+$) has been reflected well through its broad proton resonances over a wide chemical shift range δ 28 to −53 ppm due to the paramagnetic contact shift effect.[22] The paramagnetic $\mathbf{4}^+$ however fails to show the expected EPR even at 77 K both in solid and solution (acetonitrile or dichloromethane or 1:1 acetonitrile−toluene glass) states. The faster relaxation process resulting due to the strong spin−orbit coupling of Os^{III} (λ/cm^{-1}: 3000)[23] possibly contributes to the EPR silent situation as has also been noted earlier.[24]

The experimental and TD-DFT calculated electronic spectral profiles of the complexes in CH_3CN are shown in Figure 6, and the data are listed in Table 4. The complexes exhibit moderately intense multiple transitions in the UV−vis region. The higher degree of mixing of metal−ligand orbitals (covalency) due to the influence of strong spin−orbit coupling of osmium (λ = 3000 cm^{-1} [23]) has been reflected in the close by multiple electronic transitions.[25] However, TD-DFT calculations based on the DFT optimized structures of the complexes (Figure S3, Supporting Information) facilitate the assignment of the experimental transitions. The isomeric $\mathbf{1}^+$ and $\mathbf{2}^+$ can be distinguished well with special reference to the intensity of the bands, where transitions relating to $\mathbf{2}^+$ are more intense than that of $\mathbf{1}^+$. The TD-DFT calculations also suggest appreciable variations in terms of participating orbitals (Os, HL and bpy) toward the transitions in $\mathbf{1}^+$ and $\mathbf{2}^+$. The lowest energy broad and weak bands for $\mathbf{1}^+$ and $\mathbf{2}^+$ at 775 nm (DFT: 656 nm) and 696 nm (DFT: 592 nm) are assigned to ligand/metal to ligand (HL/Os → bpy) and interligand (HL → bpy) transitions, respectively. The other bpy targeted visible bands in $\mathbf{1}^+$ and $\mathbf{2}^+$ originate via metal/ligand to ligand (Os/bpy → bpy, HL/Os → bpy), metal to ligand (Os → bpy/HL), and interligand (HL → bpy), metal/ligand to ligand (Os/HL → bpy) based transitions, respectively. The higher energy UV transitions are attributed to interligand (HL → bpy) and intraligand (bpy → bpy) processes.

The moderately intense multiple visible bands in dimeric $\mathbf{3}^{2+}$ originate via metal/ligand to ligand (Os/L → bpy, Os/L/bpy → bpy) and metal to ligand (Os → bpy, Os → L) based

dx.doi.org/10.1021/ic501852a | Inorg. Chem. 2014, 53, 10695−10707

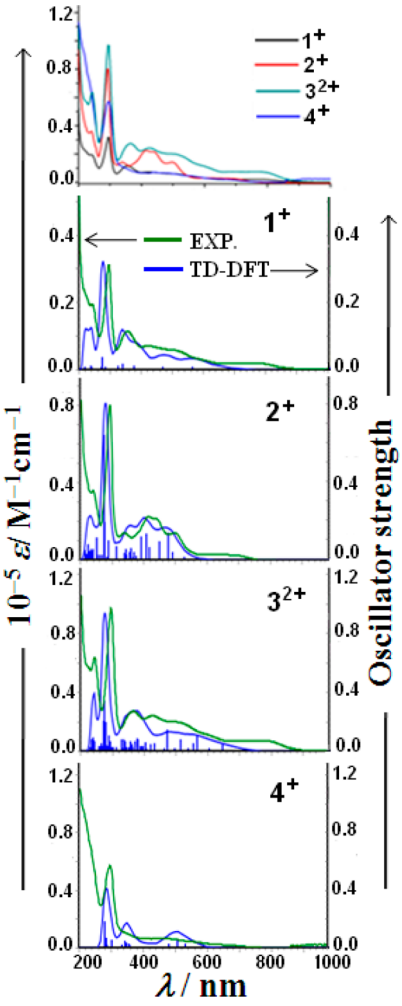

Figure 6. Experimental and TD-DFT calculated electronic spectra of $\mathbf{1}^{+}$, $\mathbf{2}^{+}$, $\mathbf{3}^{2+}$, and $\mathbf{4}^{+}$ in CH_3CN.

transitions. $\mathbf{3}^{2+}$ also displays intraligand (bpy → bpy/L → L) transitions in the UV region.

The visible energy bands of L'^{2-} derived paramagnetic complex $[Os^{III}(bpy)_2(L'^{2-})]^{+}$ ($\mathbf{4}^{+}$) are assigned to bpy targeted mixed metal/ligand to ligand (Os/L′ → bpy), ligand to ligand/metal (L′ → bpy/Os), and ligand/ligand (L′ → bpy) derived transitions.

The protonation and deprotonation processes of isomeric $[Os^{II}(bpy)_2(HL^{-})]^{+}$ with integrated O−H···N and O−H···O hydrogen bonding interactions at the back face of the coordinated HL^{-} in $\mathbf{1}^{+}$ and $\mathbf{2}^{+}$, respectively, have been explored in the pH range 0.2−12 in 1:2.5 CH_3CN−H_2O. The CH_3CN−H_2O mixed solvent is selectively chosen due to the lack of solubility of the complexes in pure water. The plots of absorbance versus pH (7.0−0.2) (Figure S4, Supporting Information) reveal the pK_a of 0.73 for $\mathbf{1}^{+}$ and <0.2 for $\mathbf{2}^{+}$ (as the lower limit of the pH-electrode is 0.2). This indeed reflects the stronger O−H···O hydrogen bonding interaction in the latter complex as compared to O−H···N in the former as has also been evidenced in their crystal structures and ^{1}H NMR spectra (see above). The pK_a values of analogous ruthenium complexes of N,N bonded HL^{-} with O−H···O hydrogen bonding interaction, $[Ru^{II}(bpy)_2(HL^{-})]^{+}$[3a] and $[Ru^{III}(acac)_2(HL^{-})]$,[3b] are reported to be <0.4 and <0.2, respectively. However, the pK_a value of $\mathbf{1}^{+}$ cannot be compared as the corresponding reference complex of N,O^{-} coordinating HL^{-} is not available. The spectral profile of $\mathbf{2}^{+}$ remains invariant in the basic region (pH 7−12) due to the effect of strong O−H···O hydrogen bonding interaction as has also been commented upon for the analogous ruthenium derivatives $[Ru^{II}(bpy)_2(HL^{-})]^{+}$[3a] and $[Ru^{III}(acac)_2(HL^{-})]$.[3b] This in turn extends the insight into the observed inertness of the N,N bonded HL^{-} in $\mathbf{2}^{+}$ to link with the second metal fragment through the available O−H···O donors. However, the plot of change in absorbance with the pH for $\mathbf{1}^{+}$ in the basic region (Figure S4, Supporting Information) gives the pK_b value of 11.55 which in essence rationalizes the fact of formation of dimeric $\mathbf{3}^{2+}$ via the activation of the O−H···N fragment of $\mathbf{1}^{+}$ by the second $\{Os^{II}(bpy)_2\}$ unit (Scheme 2).

Electrochemistry and Electronic Structures. The complexes ($\mathbf{1}^{+}$, $\mathbf{2}^{+}$, $\mathbf{3}^{2+}$, and $\mathbf{4}^{+}$) exhibit multiple redox processes in the potential range ±2.0 V versus SCE in acetonitrile (Figure 7 and Table 5). The redox processes have further been analyzed by DFT calculated molecular compositions (Table 6 and Tables S3−S18, Supporting Informations) and Mulliken spin-density plots in paramagnetic states in order to assign the electronic structural forms of the reversible redox states particularly.

The isomeric complexes $\mathbf{1}^{+}$ and $\mathbf{2}^{+}$ display similar electrochemical responses, one reversible oxidation process (Ox1), E°_{298}, V (ΔE_p, mV) at 0.21 (70) and 0.57 (80), respectively, and two successive reversible reductions (Red1 and Red2) in the potential range −1.40 to −1.80 V. The reversibility of the oxidation processes of $\mathbf{1}^{+}$ and $\mathbf{2}^{+}$ has been established by constant potential coulometry. Isomeric forms are well-distinguishable with respect to their oxidation potentials; an increase in 0.36 V oxidation potential has taken place on switching from the mixed N,O^{-} donating HL^{-} in $\mathbf{1}^{+}$ to N,N donating HL^{-} in $\mathbf{2}^{+}$. The bpy based expected reduction processes[26] have been supported by the MO compositions of LUMO ($\mathbf{1}^{+}/\mathbf{2}^{+}$), SOMO/$\alpha$-LUMO ($\mathbf{1}/\mathbf{2}$), and SOMO1 ($\mathbf{1}^{-}/\mathbf{2}^{-}$) (Table 6 and Tables S3, S5−S7, S9−S10, Supporting Information) as well as by Mulliken spin distributions in $\mathbf{1}/\mathbf{2}$ and $\mathbf{1}^{-}/\mathbf{2}^{-}$ (Table 7 and Figure S5, Supporting Information).

The mixed Os and HL derived MOs of $\mathbf{1}^{+}$ (HOMO %Os/HL, 28/60) and $\mathbf{1}^{2+}$ (β-LUMO %OS/HL/bpy, 43/33/24) (Table 5 and Tables S3−S4, Supporting Information) and Mulliken spin distribution of $\mathbf{1}^{2+}$ Os/HL = 0.677/0.326 (Table 6 and Figure 8) predict the participation of both the $\{Os(bpy)_2\}$ and HL toward the oxidation process, leading to a resonating form of $[Os^{III}(bpy)_2(HL^{-})]^{2+}$ ↔ $[Os^{II}(bpy)_2(HL^{\bullet})]^{2+}$ for $\mathbf{1}^{2+}$. However, primarily HL based MOs of $\mathbf{2}^{+}$ and $\mathbf{2}^{2+}$ (HOMO 96% HL and β-LUMO 94% HL, Table 6 and Tables S7−S8, Supporting Information) and spin density on $\mathbf{2}^{2+}$ (1.024 (HL), Table 7 and Figure 8) clearly propose exclusive involvement of HL based orbitals in the oxidation process (Ox1) which essentially extends the electronic structural form of $[Os^{II}(bpy)_2(HL^{\bullet})]^{2+}$ for $\mathbf{2}^{2+}$. It indeed demonstrates the remarkable difference in electronic structural forms of the oxidized $\mathbf{1}^{2+}$ and $\mathbf{2}^{2+}$ simply on the basis of the varying binding modes of the noninnocent HL (N,O^{-} versus N,N). Unfortunately, the oxidized species $\mathbf{1}^{2+}$ and $\mathbf{2}^{2+}$ (generated by constant potential coulometry) have failed to display any EPR response at 77 K, like the isolated paramagnetic $\mathbf{4}^{+}$ which in essence has restricted us to provide the direct experimental evidence. On oxidation of $\mathbf{1}^{+}/\mathbf{2}^{+}$ → $\mathbf{1}^{2+}/\mathbf{2}^{2+}$ (either by coulometry or by chemical oxidation using 1 equiv of cerium ammonium nitrate in acetonitrile), intensity of

dx.doi.org/10.1021/ic501852a | Inorg. Chem. 2014, 53, 10695−10707

Table 4. TD-DFT (B3LYP/CPCM/CH_3CN) Calculated Electronic Transitions for 1^+, 2^+, 3^{2+}, and 4^+

λ [nm] expt (DFT)	ε [M^{-1} cm^{-1}] (f)	transitions	character
		1^+ (S = 0)	
775 (656)	2080 (0.017)	HOMO → LUMO (0.63)	HL(π)/Os(dπ) → bpy(π^*)
503 (512)	6000 (0.022)	HOMO-2 → LUMO (0.45)	Os(dπ)/bpy(π) → bpy(π^*)
425 (400)	7190 (0.028)	HOMO → LUMO+5 (0.61)	HL(π)/Os(dπ) → bpy(π^*)
355 (355)	11 520 (0.062)	HOMO-1 → LUMO+6 (0.38)	Os(dπ) → bpy(π^*)/HL(π^*)
		HOMO-2 → LUMO+3 (0.23)	Os(dπ) → bpy(π^*)/HL(π^*)
295 (277)	31 870 (0.35)	HOMO-5 → LUMO+1 (0.38)	HL(π) → bpy(π^*)
242 (219)	19 470 (0.076)	HOMO-10 → LUMO+1 (0.36)	HL(π) → bpy(π^*)
		2^+ (S = 0)	
696 (592)	2510 (0.003)	HOMO-1 → LUMO (0.67)	HL(π) → bpy(π^*)
500 (491)	14 150 (0.040)	HOMO → LUMO+1 (0.56)	HL(π) → bpy(π^*)
		HOMO-3 → LUMO+1 (0.35)	Os(dπ)/HL(π) → bpy(π^*)
438 (452)	21 650 (0.095)	HOMO-3 → LUMO+1 (0.62)	Os(dπ)/HL(π) → bpy(π^*)
416 (409)	22 450 (0.135)	HOMO → LUMO+2 (0.50)	HL(π) → bpy(π^*)
		HOMO-3 → LUMO+2 (0.44)	Os(dπ)/HL(π) → bpy(π^*)
340 (339)	14 250 (0.035)	HOMO-3 → LUMO+5 (0.52)	Os(dπ)/HL(π) → bpy(π^*)
294 (277)	80 260 (0.194)	HOMO-2 → LUMO+8 (0.39)	HL(π) → bpy(π^*)
		HOMO-7 → LUMO+1(0.28)	bpy(π) → bpy(π^*)
240 (252)	36 060 (0.12)	HOMO-4 → LUMO+5 (0.63)	Os(dπ) → bpy(π^*)
		3^{2+}(S = 0)	
790 (648)	7180 (0.016)	HOMO-1 → LUMO+1 (0.44)	Os(dπ)/L(π) → bpy(π^*)
596 (606)	11 560 (0.018)	HOMO-2 → LUMO+2 (0.47)	Os(dπ) → bpy(π^*)
509 (555)	19 830 (0.052)	HOMO-6 → LUMO+3 (0.53)	Os(dπ)/L(π)/bpy(π) → bpy(π^*)
426 (404)	24 260 (0.058)	HOMO-4 → LUMO+4 (0.55)	Os(dπ) → L(π^*)
365 (379)	27 350 (0.085)	HOMO-6 → LUMO+2 (0.40)	Os(dπ)/L(π) → bpy(π^*)
294 (274)	97 110 (0.216)	HOMO-11 → LUMO+1 (0.22)	bpy(π) → bpy(π^*)
243 (240)	63 510 (0.093)	HOMO-13 → LUMO+4 (0.34)	L(π) → L(π^*)
		4^+ (S = $^1/_2$)	
675 (592)	2000 (0.003)	HOMO-1(β) → LUMO+1(β) (0.13)	Os(dπ)/L′(π) → bpy(π^*)
		HOMO(β) → LUMO+2(β) (0.48)	L′(π) → bpy(π^*)
558 (533)	4430 (0.026)	SOMO → LUMO(α) (0.82)	
486 (507)	6480 (0.053)	HOMO-1(α) → LUMO+1(α) (0.79)	L′(π) → bpy(π^*)
		HOMO(β) → LUMO+2(β) (0.39)	L′(π) → bpy(π^*)/Os(dπ)
440 (481)	7120 (0.028)	HOMO-2(α) → LUMO+1(β) (0.71)	Os(dπ)/L′(π) → bpy(π^*)
411 (440)	6560 (0.17)	HOMO-3(α) → LUMO(α) (0.70)	L′(π) → bpy(π^*)
		HOMO-2(α) → LUMO(α) (0.41)	Os(dπ)/L′(π) → bpy(π^*)
296 (281)	57 220 (0.185)	HOMO-7(β) → LUMO+1(β) (0.55)	L′(π) → bpy(π^*)
		HOMO-10(β) → LUMO(β) (0.39)	L′(π) → bpy(π^*)/Os(dπ)

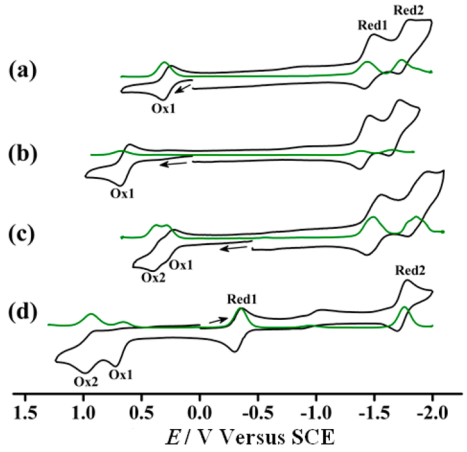

Figure 7. Cyclic voltammograms (black) and differential pulse voltammograms (green) of (a) [**1**]ClO_4, (b) [**2**]ClO_4, (c) [**3**]$(ClO_4)_2$, and (d) [**4**]ClO_4 in CH_3CN.

the bands decreases with a slight change in band positions (Figure S6, Supporting Information). The origin of the mixed metal−ligand based transitions has been assigned by TD-DFT calculations (Supporting Information Table S19).

The two close reversible oxidation processes of L^{2-} bridged diosmium(II) complex 3^{2+} appear at E^o_{298}, V (ΔE_p, mV), 0.19(70) (Ox1) and 0.29(70) (Ox2). The separation in potential (ΔE) between the successive oxidation couples (Ox2 − Ox1) of 100 mV gives the comproportionation constant (K_c) value of 49 (RT ln $K_c = nF(\Delta E)$[27]). The partial involvement of the bridge (L^{2-}) along with the metal fragment {$Os(bpy)_2$} in the oxidation processes has been revealed by the MO compositions of 3^{2+} (HOMO 76%{$Os(bpy)_2$}, 24%L), 3^{3+} (β-LUMO 74%{$Os(bpy)_2$}, 25%L; β-HOMO 79%{$Os(bpy)_2$}, 21%L) and 3^{4+} (β-LUMO 82%{$Os(bpy)_2$}, 19%L) (Table 6, Tables S11−S13, Supporting Information). This in consideration with Mulliken spin densities in paramagnetic 3^{3+} (Os1/Os2:L, 0.321/0.325:0.387) and 3^{4+} (Os1/Os2:L, 0.801/0.794:368) (Table 7, Figure 8) supports a mixed electronic configuration for the oxidized congeners: $[(bpy)_2Os^{II}(\mu\text{-}L^{2-})Os^{III}(bpy)_2]^{3+}$ (major)/$[(bpy)_2Os^{II}(\mu\text{-}L^{\bullet-})Os^{II}(bpy)_2]^{3+}$

dx.doi.org/10.1021/ic501852a | Inorg. Chem. 2014, 53, 10695−10707

Table 5. Redox Potentials and Comproportionation Constants

	E°_{298}/V (ΔE/mV)[a,b]				
complex	Ox2	Ox1	Red1	Red2	K_c[c]
$\mathbf{1}^+$		0.21(70)	−1.47(70)	−1.77(90)	
$\mathbf{2}^+$		0.57(80)	−1.44(80)	−1.68(80)	
$\mathbf{3}^{2+}$	0.29(70)	0.19(70)	−1.52(100)	−1.88(150)	4.95×10^1
$\mathbf{4}^+$	0.94[d]	0.72[d]	−0.33(60)	−1.74(90)	

[a]From cyclic voltammetry in CH_3CN/0.1 M Et_4NClO_4, scan rate 100 mV s^{-1}. [b]Potential in V versus SCE; peak potential differences ΔE_p/mV (in parentheses). [c]Comproportionation constant from $RT \ln K_c = nF(\Delta E)$. K_c between Ox1 and Ox2. [d]Irreversible process.

Table 6. DFT Calculated Selected MO Compositions for $\mathbf{1}^n$, $\mathbf{2}^n$, $\mathbf{3}^n$, and $\mathbf{4}^n$

complex	MO	fragments	% contribution
$\mathbf{1}^+$ ($S = 0$)	HOMO	Os/HL	28/60
	LUMO	bpy	91
$\mathbf{1}^{2+}$ ($S = {}^1/_2$)	β-LUMO	Os/bpy/HL	43/24/33
$\mathbf{1}$ ($S = {}^1/_2$)	SOMO	bpy	90
	α-LUMO	bpy	79
$\mathbf{1}^-$ ($S = 1$), ($E_{S=0} - E_{S=1}$ = 1000 cm^{-1})	SOMO1	bpy	78
$\mathbf{2}^+$ ($S = 0$)	HOMO	HL	96
	LUMO	bpy	91
$\mathbf{2}^{2+}$ ($S = {}^1/_2$)	β-LUMO	HL	94
$\mathbf{2}$ ($S = {}^1/_2$)	SOMO	bpy	92
	α-LUMO	bpy	85
$\mathbf{2}^-$ ($S = 1$), ($E_{S=0} - E_{S=1}$ = 1165 cm^{-1})	SOMO − 1	bpy	83
$\mathbf{3}^{2+}$ ($S = 0$)	HOMO	Os/bpy/L	52/24/24
	LUMO	bpy	88
$\mathbf{3}^{3+}$ ($S = {}^1/_2$)	β-HOMO	Os/bpy/L	56/23/21
	β-LUMO	Os/bpy/L	50/24/25
$\mathbf{3}^{4+}$ ($S = 1$), ($E_{S=0} - E_{S=1}$ = 4157 cm^{-1})	β-LUMO	Os/bpy/L	65/17/18
$\mathbf{3}^+$ ($S = {}^1/_2$)	SOMO	bpy	91
	α-LUMO	bpy	91
$\mathbf{3}$ ($S = 1$), ($E_{S=0} - E_{S=1}$ = 3517 cm^{-1})	SOMO − 1	bpy	92
$\mathbf{4}^+$ ($S = {}^1/_2$)	β -HOMO	L′	84
	β-LUMO	Os/bpy/L′	37/44/19
$\mathbf{4}$ ($S = 0$), ($E_{S=1} - E_{S=0}$ = 7216 cm^{-1})	HOMO	Os/bpy/L′	45/29/27
	LUMO	bpy	90
$\mathbf{4}^-$ ($S = {}^1/_2$)	SOMO	bpy	99

Table 7. DFT Calculated Mulliken Spin Distributions for $\mathbf{1}^n$, $\mathbf{2}^n$, $\mathbf{3}^n$, and $\mathbf{4}^n$

complex	Os	HL/L/L′	bpy
$\mathbf{1}^{2+}$ ($S = {}^1/_2$)	0.677	0.326	−0.006
$\mathbf{1}$ ($S = {}^1/_2$)	−0.086	0.005	1.0087
$\mathbf{1}^-$ ($S = 1$), ($E_{S=0} - E_{S=1}$ = 1000 cm^{-1})	0.188	0.039	1.771
$\mathbf{2}^{2+}$ ($S = {}^1/_2$)	−0.010	1.024	−0.001
$\mathbf{2}$ ($S = {}^1/_2$)	−0.075	0.008	1.068
$\mathbf{2}^-$ ($S = 1$), ($E_{S=0} - E_{S=1}$ = 1165 cm^{-1})	0.138	0.022	1.84
$\mathbf{3}^{3+}$ ($S = {}^1/_2$)	0.646	0.387	−0.033
$\mathbf{3}^{4+}$ ($S = 1$), ($E_{S=0} - E_{S=1}$ = 4157 cm^{-1})	1.595	0.368	0.018
$\mathbf{3}^+$ ($S = {}^1/_2$)	−0.065	−0.005	1.066
$\mathbf{3}$ ($S = 1$), ($E_{S=0} - E_{S=1}$ = 3517 cm^{-1})	−0.195	−0.008	2.199
$\mathbf{4}^+$ ($S = {}^1/_2$)	0.715	0.222	0.064
$\mathbf{4}^-$ ($S = {}^1/_2$)	−0.164	−0.026	1.186

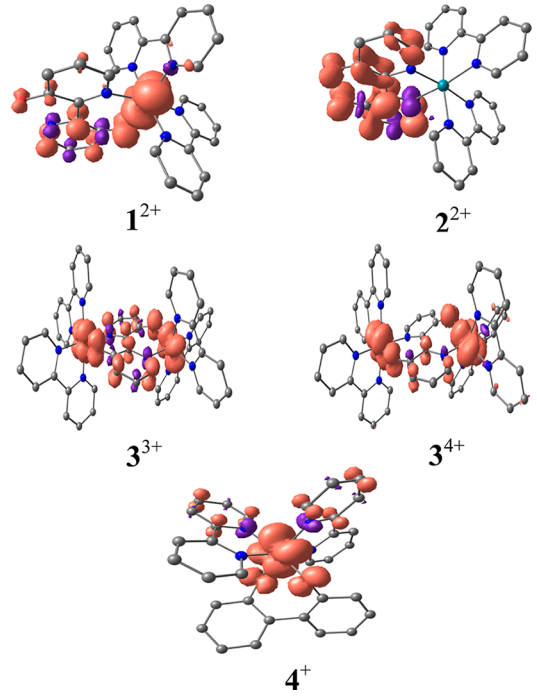

Figure 8. Selected Mulliken spin density plots of $\mathbf{1}^n$, $\mathbf{2}^n$, $\mathbf{3}^n$, and $\mathbf{4}^n$.

(minor) ($\mathbf{3}^{3+}$) and $[(bpy)_2Os^{III}(\mu\text{-}L^{2-})Os^{III}(bpy)_2]^{4+}$ (major)/$[(bpy)_2Os^{II}(\mu\text{-}L^{\bullet-})Os^{III}(bpy)_2]^{4+}$ (minor) ($\mathbf{3}^{4+}$). The K_c value of 49 for the mixed valent $Os^{II}Os^{III}$ state in $\mathbf{3}^{3+}$ implies the bridge (L^{2-}) mediated virtually no intermetallic electrochemical coupling as expected from a typical class I system.[23b,28] This has also been reflected in the almost equal spin densities on the two osmium centers in $\mathbf{3}^{3+}$ (Os1/Os2:0.321/0.325, Figure 8 and Table 7). The small separation of 100 mV between the successive oxidation processes (Ox1/Ox2) in $\mathbf{3}^{2+}$ has prevented us from checking the spectral features of the oxidized congeners ($\mathbf{3}^{3+}/\mathbf{3}^{4+}$) either by coulometry or by stepwise chemical oxidations using cerium ammonium nitrate in acetonitrile. The two bpy based successive reductions have been corroborated by the bpy dominated MOs as well as spins in $\mathbf{3}^+$ (Red1) and $\mathbf{3}$ (Red2) (Tables 6 and 7 and Tables S14 and S15 as well as Figure S5, Supporting Information).

The calculated Mulliken spin density distribution of Os/L′ = 0.715/0.22 (Table 7 and Figure 8) for the paramagnetic complex $\mathbf{4}^+$ suggests that it can be best described as a resonating form of $[Os^{III}(bpy)_2(L'^{2-})]^+ \leftrightarrow [Os^{II}(bpy)_2(L^{\bullet-})]^+$. The two unequal C−O bond lengths of L′ in $\mathbf{4}^+$ (approximate difference between the two C−O bond lengths of L′ in each molecule of $\mathbf{4}^+$ is 0.03 Å, see above) also support the aforesaid electronic form. Complex $\mathbf{4}^+$ exhibits two close by irreversible oxidations, E_{pa} at 0.72 (Ox1) and 0.94 (Ox2), and two reversible reductions (Red1 and Red2) (Figure 7 and Table 5)

dx.doi.org/10.1021/ic501852a | Inorg. Chem. 2014, 53, 10695−10707

Scheme 5. Electronic Structural Forms of 1^n–4^n

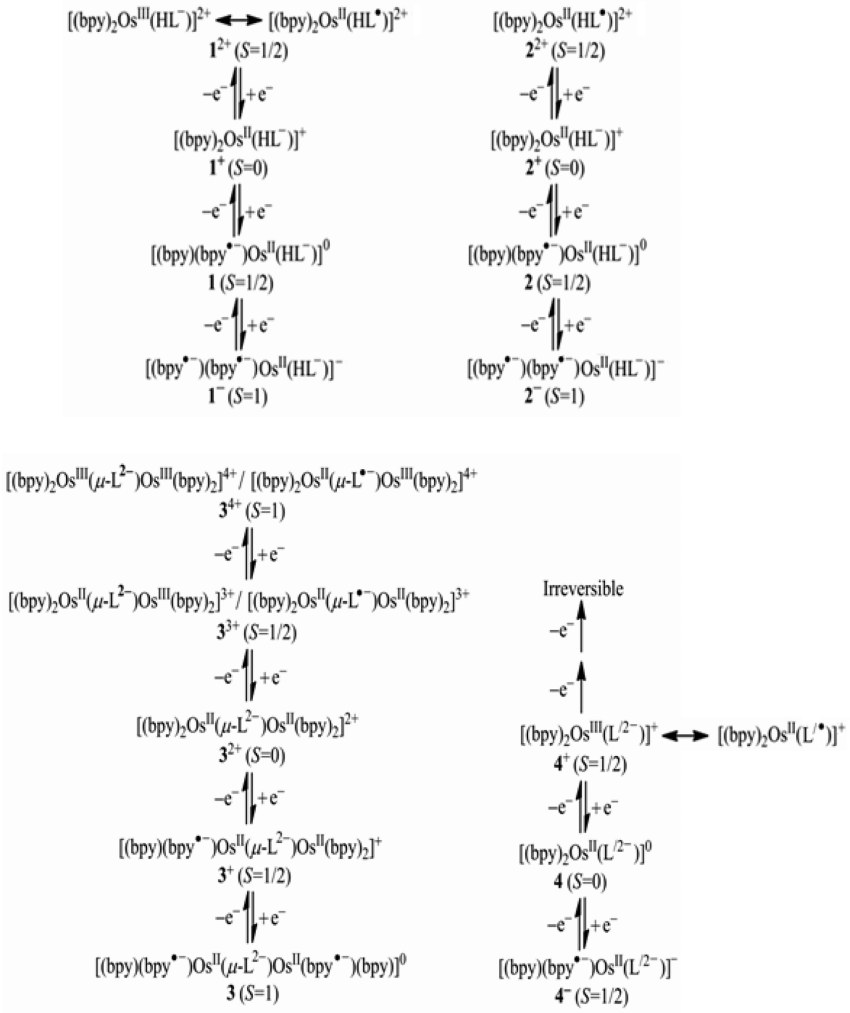

in cyclic voltammetric time scale. The $\{Os(bpy)_2\}$ dominated β-LUMO of 4^+ (81%) and HOMO of **4** (74%) (Table 6 and Tables S16–S17, Supporting Information) are supportive of the electronic configuration of $[Os^{II}(bpy)_2(L'^{2-})]$ for the first reduced (Red 1) state (**4**). An enhancement of 0.54 V of Os^{II}/Os^{III} couple has taken place on moving from a dianionic L'^{2-} derived 4^+ to monoanionic HL^- based 1^+. The MO compositions of **4** (LUMO, 90% bpy) and 4^- (SOMO, 99% bpy) (Table 5 and Tables S17–S18, Supporting Information) and Mulliken spin density of 4^- (bpy 1.186, Table 6, Figure S5, Supporting Information) however imply bpy targeted second reduction (Red 2).

The electronic structural forms of 1^n–4^n are depicted in Scheme 5.

CONCLUSION

The following statements are the salient points of the article: (1) The selective use of $\{Os^{II}(bpy)_2\}$ metal fragment stabilizes the hitherto unrecognized N,O$^-$ coordination mode of the monodeprotonated 2,2′-bipyridine-3,3′-diol (H_2L) with O–H···N hydrogen bonding interaction at its back face in 1^+ along with the isomeric complex 2^+ encircling well established N,N bonded HL^- with O–H···O hydrogen bond. (2) The isomeric 1^+ and 2^+ exhibit distinctive structural, spectral, electrochemical, and pH driven processes. (3) Though facile activation of the moderately strong O–H···N hydrogen bond in 1^+ by the second unit of $\{Os^{II}(bpy)_2\}$ yields the deprotonated L^{2-} bridged $[(bpy)_2Os^{II}(\mu\text{-}L^{2-})Os^{II}(bpy)_2]^{2+}$ (3^{2+}), $\{Os^{II}(bpy)_2\}$ fails to activate the O–H···O function in 2^+. (4) Isomeric 1^+ and 2^+ exhibit remarkable difference with respect to the involvement of metal or HL^- or mixed metal/HL^- based orbitals toward the oxidation process, leading to the electronic structural forms of $[Os^{III}(bpy)_2(HL^-)]^{2+} \leftrightarrow [Os^{II}(bpy)_2(HL^\bullet)]^{2+}$ and $[Os^{II}(bpy)_2(HL^\bullet)]^{2+}$ for 1^{2+} and 2^{2+}, respectively. (5) The deprotonated L^{2-} bridged $[(bpy)_2Os^{II}(\mu\text{-}L^{2-})Os^{II}(bpy)_2]^{2+}$ (3^{2+}) exhibits virtually no intermetallic electrochemical coupling (K_c= 49) at the mixed valent $Os^{II}Os^{III}$ state (class I). Further, the partial involvement of L^{2-} along with the metal ion leads to the mixed electronic structural forms for the successive oxidation processes in 3^{3+} and 3^{4+}. (6) The deprotonated 2,2′-biphenol (H_2L') in paramagnetic $[Os^{III}(bpy)_2(L'^{2-})]^+$ (4^+) forms a relatively less known twisted seven-membered chelate, and its electronic structural form can be best represented as a resonance form of $[Os^{III}(bpy)_2(L'^{2-})]^+ \leftrightarrow [Os^{II}(bpy)_2(HL^{\bullet-})]^+$.

EXPERIMENTAL SECTION

Materials. The precursor complexes *cis*-$Os(bpy)_2(Cl)_2$[29] and the ligand 2,2′-bipyridine-3,3′-diol (H_2L)[30] were prepared according to the reported literature procedures. The ligand 2,2′-biphenol (H_2L') was purchased from Merck. All other chemicals were reagent grade,

dx.doi.org/10.1021/ic501852a | Inorg. Chem. 2014, 53, 10695–10707

and for spectroscopic, electrochemical studies, HPLC grade solvents were used.

Physical Measurements. The electrical conductivities of the complexes in CH_3CN were checked by using Systronic 305 conductivity bridge. ^1H NMR spectra were recorded using Bruker Avance III 500 MHz spectrometer for $\mathbf{1}^+$, $\mathbf{3}^{2+}$, and $\mathbf{4}^+$ and Bruker Avance III 400 MHz spectrometer for $\mathbf{2}^+$. FT-IR spectra were recorded on a Nicolet spectrophotometer with samples prepared as KBr pellets. Cyclic voltammetry measurements were performed on a PAR model 273A electrochemistry system. Glassy carbon working electrode, platinum wire auxiliary electrode, and a saturated calomel reference electrode (SCE) were used in a standard three-electrode configuration cell. A platinum wire-gauze working electrode was used for the constant potential coulometry experiment. Tetraethylammonium perchlorate (TEAP) was used as the supporting electrolyte, and concentration of the solution was taken as 10^{-3} M; the scan rate used was 100 mV s^{-1}. All electrochemical experiments were carried out under dinitrogen atmosphere. The half-wave potential E°_{298} was set equal to $0.5(E_{pa} + E_{pc})$, where E_{pa} and E_{pc} are anodic and cathodic cyclic voltammetry peak potentials, respectively. UV−vis−NIR spectral studies were performed on a PerkinElmer Lambda 950 spectrophotometer. The elemental analyses were carried out on a Thermoquest (EA 1112) microanalyzer. Electrospray mass spectra (ESI-MS) were recorded on a Bruker's Maxis Impact (282001.00081).

Crystallography. Single crystals of $[\mathbf{1}]ClO_4$, $[\mathbf{2}]ClO_4$, and $[\mathbf{3}](ClO_4)_2$ were grown by slow evaporation of their 1:1 dichloromethane−toluene solution. The single crystals of $[\mathbf{4}]ClO_4$ were grown from its 1:1 methanol−chloroform solution. X-ray crystal data were collected on RIGAKU SATURN-724 CCD single crystal X-ray diffractometer. Data collection was evaluated by using the CrystalClear-SM Expert software. The data were collected by the standard ω scan techniques. The structures were solved by direct method using SHELXS-97 and refined by full matrix least-squares with SHELXL-97, refining on F^2.[31] All non-hydrogen atoms were refined anisotropically. The hydrogen atoms were placed in geometrically constrained positions and refined with isotropic temperature factors, generally $1.2U_{eq}$ of their parent atoms. Hydrogen atoms were included in the refinement process as per the riding model. Hydrogen atoms associated with the solvent water molecules in $[\mathbf{3}](ClO_4)_2$ could not be located; however, these have been considered for the empirical formula in Table 1. The disordered solvent molecules in $[\mathbf{1}]ClO_4$ and $[\mathbf{2}]ClO_4$ were SQUEEZE by PLATON[32] program.

Computational Details. Full geometry optimizations were carried out by using the density functional theory method at (R)B3LYP and (U)B3LYP levels for $\mathbf{1}^+$, $\mathbf{2}^+$, $\mathbf{3}^{2+}$, **4** and $\mathbf{1}^{2+}$, **1**, $\mathbf{1}^-$, $\mathbf{2}^{2+}$, **2**, $\mathbf{2}^-$, $\mathbf{3}^{3+}$, $\mathbf{3}^{4+}$, $\mathbf{3}^+$, **3**, $\mathbf{4}^+$, $\mathbf{4}^-$, respectively.[33] Except osmium all other elements were assigned the 6-31G* basis set. The LANL2DZ basis set with effective core potential was employed for the osmium atom.[34] The vibrational frequency calculations were performed to ensure that the optimized geometries represent the local minima, and there are only positive eigenvalues. All calculations were performed with *Gaussian09* program package.[35] Vertical electronic excitations based on (R)B3LYP/(U)B3LYP optimized geometries were computed for $\mathbf{1}^n$ (n = +1, +2), $\mathbf{2}^n$ (n = +1, +2), $\mathbf{3}^n$ (n = +2), and $\mathbf{4}^+$ using the time-dependent density functional theory (TD-DFT) formalism[36] in acetonitrile using conductor-like polarizable continuum model (CPCM).[37] *Chemissian 1.7*[38] was used to calculate the fractional contributions of various groups to each molecular orbital. All calculated structures were visualized with *ChemCraft*.[39]

Cerium Ammonium Nitrate (CAN) Titrations. The acetonitrile solution of CAN (1×10^{-3} M) was gradually added to the acetonitrile solution of $\mathbf{1}^+/\mathbf{2}^+$ (1×10^{-5} M) up to 1 equiv, in a cuvette with 1 cm light path length. The absorption spectral changes were monitored after each addition. Each absorption spectrum was plotted on appropriate consideration of the volume change on addition of CAN solution.

Synthesis of Isomeric $[Os^{II}(bpy)_2(HL^-)]ClO_4$ ([1]ClO_4 and [2]ClO_4). The precursor complex $Os(bpy)_2(Cl)_2$ (100 mg, 0.17 mmol), the ligand 2,2′-bipyridine-3,3′-diol (H_2L) (38 mg, 0.20 mmol), and freshly distilled (over KOH) triethylamine (44 mg, 0.44 mmol) were taken in 40 mL 1:1 ethanol−water. The reaction mixture was refluxed under dinitrogen atmosphere for 36 h. The initial brown color was gradually changed to reddish brown. The solvent was then removed under reduced pressure, and the compound was redissolved in 5 mL of acetonitrile. The addition of saturated aqueous solution of sodium perchlorate to the above acetonitrile solution resulted in dark precipitation. It was then filtered, and the solid mass was washed thoroughly by ice-cold water and dried under vacuum. The crude product was purified by using a neutral alumina column which led to the initial elution of the reddish complex $[\mathbf{1}]ClO_4$ followed by yellowish complex $[\mathbf{2}]ClO_4$ by dichloromethane−acetonitrile (4:1) solvent mixture. Evaporation of the solvent under reduced pressure yielded pure solid complexes $[\mathbf{1}]ClO_4$ and $[\mathbf{2}]ClO_4$ which were further dried under vacuum. Details follow or $[\mathbf{1}]ClO_4$. Yield: 45 mg (33%). ^1H NMR in $CDCl_3$ [δ/ppm (J /Hz)]: 17.00 (s, broad, 1H), 9.0 (d, 5.4, 1H), 8.74 (d, 8.24, 1H), 8.55 (d, 8.12, 1H), 8.19 (t, 7.58, 2H), 7.85 (t, 7.84, 1H), 7.67 (m, 2H), 7.45 (m, 5H), 7.29 (m, 1H), 7.11 (m, 2H), 6.96 (m, 2H), 6.86(t, 6.08, 1H), 6.77 (d, 7.12, 1H), 6.66 (m, 1H), 6.37(d, 4.48, 1H). MS (ESI+, CH_3CN): m/z {[M]$^+$} calcd 691.1415; found 691.1357. Molar conductivity (CH_3CN): Λ_M = 92 Ω^{-1} cm^2 M^{-1}. Anal. Calcd for $C_{30}H_{23}ClN_6O_6Os$: C, 45.66; H, 2.94; N, 10.65. Found: C, 45.34; H, 2.77; N, 10.42%. $\nu(ClO_4^-, cm^{-1})$: 1089.

Details follow or $[\mathbf{2}]ClO_4$. Yield: 35 mg (26%). ^1H NMR in $CDCl_3$ [δ/ppm (J/Hz)]: 18.21 (s, 1H), 8.60 (t, 9.05, 2H), 7.79 (t, 7.62, 2H), 7.65 (d, 5.3, 1H), 7.55 (d, 5.5, 1H), 7.28 (m, 2H), 6.99 (d, 7.2, 1H), 6.80 (m, 1H), 6.60 (d, 5.25, 1H). MS (ESI+, CH_3CN): m/z {[M]$^+$} calcd 691.1415; found 691.1357. Molar conductivity (CH_3CN): Λ_M = 98 Ω^{-1} cm^2 M^{-1}. Anal. Calcd for $C_{30}H_{23}ClN_6O_6Os$: C, 45.66; H, 2.94; N, 10.65%. Found: C, 45.28; H, 2.74; N, 10.48%. $\nu(ClO_4^-, cm^{-1})$: 1092.

Synthesis of $[(bpy)_2Os^{II}(\mu\text{-}L^{2-})Os^{II}(bpy)_2)](ClO_4)_2$ ([3]$(ClO_4)_2$). The mononuclear complex $\mathbf{1}^+$ (100 mg, 0.13 mmol), the precursor complex $Os(bpy)_2(Cl)_2$ (92 mg, 0.16 mmol) and freshly distilled (over KOH) triethylamine (40 mg, 0.40 mmol) were taken in 40 mL 1:1 ethanol−water. The mixture was heated to reflux under dinitrogen atmosphere for 20 h. The solution was dried under reduced pressure and redissolved in 5 mL of acetonitrile. Saturated aqueous solution of sodium perchlorate was then added to the above acetonitrile solution which spontaneously yielded dark precipitation of the compound. The filtered solid mass was washed thoroughly with ice-cold water and dried under vacuum. The crude product was purified on a neutral alumina column, and the pure brown complex was eluted by 1:5 dichloromethane−acetonitile mixture. The pure complex $[\mathbf{3}](ClO_4)_2$ in the solid form was obtained on removal of the solvent under reduced pressure. Yield: 140 mg (80%).

Alternate Procedure. The dimeric complex $[\mathbf{3}](ClO_4)_2$ was also prepared directly from the ligand H_2L and $Os(bpy)_2(Cl)_2$. The mixture of the precursor complex $Os(bpy)_2(Cl)_2$ (100 mg, 0.17 mmol), the ligand 2,2′-bipyridine-3,3′-diol (H_2L) (10 mg, 0.053 mmol), and freshly distilled (over KOH) triethylamine (13 mg, 0.13 mmol) in 40 mL 1:1 ethanol−water was refluxed under dinitrogen atmosphere for 36 h. The dried product was dissolved in 5 mL acetonitrile and precipitated out by adding saturated aqueous sodium perchlorate solution. The precipitate was filtered and washed thoroughly by ice-cold water and dried under vacuum. The product was purified by using a neutral alumina column and 1:5 dichloromethane−acetonitile mixture as eluant. Yield: 44 mg (54%).

Details follow or $[\mathbf{3}](ClO_4)_2$. ^1H NMR in CD_3CN [δ/ppm (J/Hz)]: 8.86 (d, 5.25, 1H), 8.56 (d, 6.72, 2H), 8.41 (d, 8.25, 1H), 8.26 (t, 8.07, 2H), 7.96 (d, 5.8, 1H), 7.80 (t, 6.15, 1H), 7.50 (t, 7.85, 1H), 7.42 (m, 4H), 7.34 (t, 5.4, 1H), 7.03 (d, 5.85. 1H), 6.92 (m, 2H), 6.1 (m, 1H), 6.03 (m, 1H). MS (ESI+, CH_3CN): m/z {[M^{2+}/2]} calcd 596.1169; found 596.1450. Molar conductivity (CH_3CN): Λ_M = 222 Ω^{-1} cm^2 M^{-1}. Anal. Calcd for $C_{50}H_{38}Cl_2N_{10}O_{10}Os_2$: C, 43.20; H, 2.76; N, 10.08. Found: C, 43.48; H, 2.67; N, 9.9%. $\nu(ClO_4^-, cm^{-1})$: 1092.

Synthesis of $[Os^{III}(bpy)_2(L'^{2-})]ClO_4$ ([4]ClO_4). The mixture of precursor complex $Os(bpy)_2(Cl)_2$ (100 mg, 0.17 mmol), the ligand 2,2′-biphenol (H_2L', 38 mg, 0.20 mmol), and freshly distilled triethylamine (over KOH) (40 mg, 0.40 mmol) in 50 mL 1:1 ethanol−water was heated to reflux for 30 h under dinitrogen

dx.doi.org/10.1021/ic501852a | *Inorg. Chem.* 2014, 53, 10695−10707

atmosphere. The solution was evaporated to dryness under reduced pressure. The resulting solid mass in 5 mL of acetonitrile was added to saturated aqueous sodium perchlorate solution. The precipitate thus obtained was filtered and washed thoroughly with ice-cold water. The product was purified on a neutral alumina column, and 5:1 dichloromethane−acetonitrile solution was used as eluant. Evaporation of the solvent under reduced pressure yielded the pure complex [**4**]ClO_4 which was further dried under vacuum. Yield: 96 mg (70%). ^{1}H NMR in $CDCl_3$ [δ/ppm (J/Hz)]: 28.24 (s, 1H), 24.07 (s, 1H), 22.97 (s, 1H), 13.01 (s, 1H), 9.17 (s, 1H), 7.83 (s, 1H), 7.30 (s, 1H), −5.79 (s, 1H), −12.70 (s, 1H), −29.51 (s, 1H), −32.08 (s, 1H), −52.8 0 (s,1H). MS (ESI+, CH_3CN): m/z {[M]$^+$} calcd 688.1472; found 688.1291. Molar conductivity (CH_3CN): Λ_M = 103 Ω^{-1} cm^2 M^{-1}. Anal. Calcd for $C_{32}H_{24}ClN_4O_6Os$: C, 48.89; H, 3.08; N, 7.13. Found: C, 48.64; H, 2.93; N, 7.51%. ν(ClO_4^-, cm^{-1}): 1086.

■ ASSOCIATED CONTENT

Supporting Information

X-ray crystallographic files in CIF format for [**1**]ClO_4 (CCDC No. 1016747), [**2**]ClO_4, (CCDC No. 1016748), [**3**]$(ClO_4)_2$ (CCDC No. 1016749), and [**4**]ClO_4 (CCDC No. 1016750); mass spectra (Figure S1), ORTEP of [**4**]ClO_4 (Figure S2); DFT optimized structures (Figure S3); electronic spectra of $\mathbf{1}^+/\mathbf{2}^+$ as a function of pH (Figure S4); spin density plots (Figure S5); electronic spectra of $\mathbf{1}^{2+}/\mathbf{2}^{2+}$ (Figure S6); structural parameters (Tables S1−S2); MO compositions (Tables S3−S18); spectral data and TD-DFT calculations for $\mathbf{1}^{2+}$ and $\mathbf{2}^{2+}$ (Table S19). This material is available free of charge via the Internet at http://pubs.acs.org.

■ AUTHOR INFORMATION

Corresponding Author

*E-mail: lahiri@chem.iitb.ac.in. Phone: +91 22 25767159. Fax: +91 22 25723480.

Notes

The authors declare no competing financial interest.

■ ACKNOWLEDGMENTS

Financial support received from the Department of Science and Technology, Council of Scientific and Industrial Research (fellowship to P.G. and A.D.) and University Grants Commission (fellowship to R.R.), New Delhi (India) is gratefully acknowledged.

■ REFERENCES

(1) (a) Giordino, P. J.; Bock, C. K.; Wrighton, M. S. *J. Am. Chem. Soc.* **1978**, *100*, 6960−6965. (b) Haga, M. *Inorg. Chim. Acta* **1983**, *75*, 29−35. (c) Kundu, T.; Mobin, S. M.; Lahiri, G. K. *Dalton Trans.* **2010**, *39*, 4232−4242. (d) Das, A.; Kundu, T.; Mobin, S. M.; Priego, J. S.; Jimenez-Aparicio, R.; Lahiri, G. K. *Dalton Trans.* **2013**, *42*, 13733−13746. (e) Kundu, T.; Chowdhury, A. D.; De, D.; Mobin, S. M.; Purnaik, V. G.; Datta, A.; Lahiri, G. K. *Dalton Trans.* **2012**, *41*, 4484−4496. (f) Dubois, M. R.; Dubois, D. L. *Chem. Soc. Rev.* **2009**, *38*, 62−72. (g) DesPasquale, J.; Nieto, I.; Reuther, L. E.; Herbst-Gervasoni, C. J.; Paul, J. J.; Mochalin, V.; Zeller, M.; Thomas, C. M.; Addison, A. W. *Inorg. Chem.* **2013**, *52*, 9175−9183. (h) Himeda, Y. *Eur. J. Inorg. Chem.* **2007**, 3927−3941. (i) Coles, P. M.; Aragon-Saez, P. J.; Hitchcock, P. B.; Davidson, M. G.; Maksic, Z. B.; Vianello, R.; Leito, I.; Kalijurand, I.; Apperley, D. C. *J. Am. Chem. Soc.* **2009**, *131*, 16858−16868.

(2) (a) Kunkely, H.; Vogler, A. *Inorg. Chim. Acta* **2003**, *343*, 357−360. (b) Bugarcic, T.; Habtemariam, A.; Stepankova, J.; Heringova, P.; Kasparkova, J.; Deeth, R. J.; Johnstone, R. D. L.; Prescimone, A.; Parkin, A.; Parsons, S.; Brabec, V.; Sadler, P. J. *Inorg. Chem.* **2008**, *47*, 11470−11486.

(3) (a) Thompson, A. M. W. C.; Jeffery, J. C.; Liard, D. J.; Ward, M. D. *J. Chem. Soc., Dalton Trans.* **1996**, 879−884. (b) Ghosh, P.; Mondal, P.; Ray, R.; Das, A.; Bag, S.; Mobin, S. M.; Lahiri, G. K. *Inorg. Chem.* **2014**, *53*, 6094−6106.

(4) (a) Li, H.; Hou, C.; Shi, J.-M.; Zhang, S.-G. *J. Coord. Chem.* **2008**, *61*, 3501−3507. (b) Hou, C.; Shi, J.-M.; Sun, Y.-M.; Shi, W.; Cheng, P.; Liu, L.-D. *Dalton Trans.* **2008**, 5970−5976. (c) Stephenson, M. D.; Hardie, M. J. *CrystEngComm* **2007**, *9*, 496−502. (d) Jung, O-. S.; Kim, Y. T.; Lee, Y-. A.; Kim, Y. J.; Chae, H. K. *Inorg. Chem.* **1999**, *38*, 5457−5460.

(5) Himeda, Y.; Komatsuzaki, N. O.; Sugihara, H.; Kasuga, K. *Organometallics* **2007**, *26*, 702−712.

(6) Mendivil, E. T.; Diez, J.; Cadierno, V. *Catal. Sci. Technol.* **2011**, *1*, 1605−1615.

(7) Zhang, S. G.; Hou, C. *Acta Crystallogr.* **2008**, *E64*, m1131.

(8) Li, M. J. *J. Chem. Crystallogr.* **2009**, *39*, 143−146.

(9) (a) Santra, B. K.; Thakur, G. A.; Ghosh, P.; Pramanik, A.; Lahiri, G. K. *Inorg. Chem.* **1996**, *35*, 3050−3052. (b) Das, D.; Mondal, T. K.; Mobin, S. M.; Lahiri, G. K. *Inorg. Chem.* **2009**, *48*, 9800−9810. (c) Maji, S.; Sarkar, B.; Mobin, S. M.; Fiedler, J.; Kaim, W.; Lahiri, G. K. *Dalton Trans.* **2007**, 2412−2418.

(10) (a) Taube, H. *Angew. Chem., Int. Ed. Engl.* **1984**, *23*, 329−339. (b) Richardson, D. E.; Sen, J. P.; Bhur, J. D.; Taube, H. *Inorg. Chem.* **1982**, *21*, 3136−3140. (c) Dubici, L.; Ferguson, J.; Krausz, E. R.; Lay, P. A.; Maeder, M.; Magnuson, R. H.; Taube, H. *J. Am. Chem. Soc.* **1985**, *107*, 2167−2171. (d) Lay, P. A.; Magnuson, R. H.; Taube, H. *Inorg. Chem.* **1988**, *27*, 2364−2371. (e) Magnuson, R. H.; Lay, P. A.; Taube, H. *J. Am. Chem. Soc.* **1983**, *105*, 2507−2509.

(11) (a) Cotton, F. A.; Wilkinson, G.; Murillio, C. A.; Bochmann, M. *Advanced Inorganic Chemistry*, 6th ed.; Wiley Publishing: Chichester, U.K., 1999; pp 27−29. (b) Huheey, J. E.; Keiter, E. A.; Keiter, R. L. *Inorganic Chemistry, Principles of Structure and Reactivity*, 4th ed.; Harper Collins College Publishing: New York, 1993; pp 522−524.

(12) (a) Griffith, W. P.; Nogueira, H. I. S.; White, A. J. P.; Williams, D. J. *Polyhedron* **1997**, *16*, 1323−1329. (b) Levson, W.; Patel, B.; Reid, G.; Ward, A. J. *J. Organomet. Chem.* **2001**, *619*, 218−225. (c) Alguindigue, S. S.; Khan, M. A.; Ashby, M. T. *Organometallics* **1999**, *18*, 5112−5119. (d) Sarper, O.; Sarkar, B.; Fiedler, J.; Lissner, F.; Kail, W. *Inorg. Chim. Acta* **2010**, *363*, 3070−3077. (e) Lin, J.-H.; Che, C.-M.; Lai, T.-F.; Poon, C.-K.; Cui, X. *J. Chem. Soc., Chem. Commun.* **1991**, *7*, 468−470.

(13) Laye, R. H.; Bell, Z. R.; Ward, M. D. *New J. Chem.* **2003**, *27*, 684−691.

(14) Lahiri, G. K.; Bhbattacharya, S.; Ghosh, B. K.; Chakravorty, A. *Inorg. Chem.* **1987**, *26*, 4324−4331.

(15) (a) Gilli, P.; Bertolasi, V.; Ferreti, V.; Gilli, G. *J. Am. Chem. Soc.* **1994**, *116*, 909−915. (b) Emsely, J. *Chem. Soc. Rev.* **1980**, *9*, 91−124. (c) Novak, A. *Struct. Bonding (Berlin)* **1974**, *18*, 177−216. (d) Speakman, J. C. *Struct. Bonding (Berlin)* **1974**, *12*, 141−199. (e) Beijer, F. H.; Kooijman, H.; Spek, A. L.; Sijbesma, R. P.; Meijer, E. W. *Angew. Chem., Int. Ed.* **1998**, *37*, 75−78. (f) Arunan, E.; Desiraju, G. R.; Klein, R. A.; Sadlej, J.; Scheiner, S.; Alkorta, I.; Clary, D. C.; Carbtree, R. H.; Dannenberg, J. J.; Hobza, P.; Kjaergaard, H. G.; Legon, A. C.; Mennucci, B.; Nebitt, D. J. *Pure Appl. Chem.* **2011**, *83*, 1637−1641.

(16) Constable, E. C.; Raithby, P. R.; Smit, D. N. *Polyhedron* **1989**, *8*, 367−369.

(17) Basuli, F.; Peng, S-. M.; Bhattacharya, S. *Polyhedron* **1999**, *18*, 391−402.

(18) Samanta, R.; Munshi, P.; Santra, B. K.; Loknath, N. K.; Sridhar, M. A.; Prasad, J. S.; Lahiri, G. K. *J. Organomet. Chem.* **1999**, *579*, 311−320.

(19) Demandis, K. D.; Dattelbaum, D. M.; Kober, E. M.; Concepcion, J. J.; Paul, J. J.; Meyer, T. J.; White, P. S. *Inorg. Chim. Acta* **2007**, *360*, 1143−1153.

(20) Xing, J.; Man, W.-L.; Yiu, S.-M.; Peng, S.-M.; Lau, T.-C. *Chem.—Eur. J.* **2011**, *17*, 13044−13051.

(21) Li, W.-K.; Zhou, G.-D.; Mak, T. C. W. M. *Advanced Structural Inorganic Chemistry*; Oxford Publishing: New York, 2008; pp 403−416.

(22) (a) Koiwa, T.; Masuda, Y.; Shono, J.; Kawamoto, Y.; Hoshino, Y.; Hashimoto, T.; Natarajan, K.; Shimizu, K. *Inorg. Chem.* **2004**, *43*, 6215−6223. (b) Eaton, D. R. *J. Am. Chem. Soc.* **1965**, *87*, 3097−3102. (c) Palmer, R. A.; Fay, R. C.; Piper, T. S. *Inorg. Chem.* **1964**, *3*, 875−881. (d) Holm, R. H.; Cotton, F. A. *J. Am. Chem. Soc.* **1958**, *80*, 5658−5663. (e) Fay, R. C.; Piper, T. S. *J. Am. Chem. Soc.* **1963**, *85*, 500−504. (f) Chen, J.-L.; Zhang, X.-U.; Zhang, L.-Y.; Shi, L.-X.; Chen, Z.-N. *Inorg. Chem.* **2005**, *44*, 1037−1043. (g) Das, A.; Sacherer, T.; Maji, S.; Mondal, T. K.; Mobin, S. M.; Urbanos, F. A.; Jimenez-Aparicio, R.; Kaim, W.; Lahiri, G. K. *Inorg. Chem.* **2011**, *50*, 7040−7049. (h) Kumbhakar, D.; Sarkar, B.; Maji, S.; Mobin, S. M.; Fiedler, J.; Urbanos, F. A.; Jimenez-Aparicio, R.; Kaim, W.; Lahiri, G. K. *J. Am. Chem. Soc.* **2008**, *130*, 17575−17583.

(23) (a) Weil, J. A.; Bolton, J. R.; Wertz, J. E. *Electron Paramagnetic Resonance*; Wiley Publishing: New York, 1994; p 532. (b) Das, A.; Agarwala, H.; Kundu, T.; Ghosh, P.; Mondal, S.; Mobin, S. M.; Lahiri, G. K. *Dalton Trans.* **2014**, *43*, 13932−13947.

(24) Sarkar, B.; Kaim, W. *Coord. Chem. Rev.* **2013**, *257*, 1650−1659.

(25) Concepcion, J. J.; Dattelbaum, M. D.; Meyer, T. J.; Rocha, R. C. *Philos. Trans. R. Soc. London* **2008**, *366*, 163−175.

(26) (a) Ghumann, S.; Sarkar, B.; Patra, S.; Parimal, K.; Salgeren, J. V.; Fiedler, J.; Kaim, W.; Lahiri, G. K. *Dalton Trans.* **2005**, 706−712. (b) Roffia, S.; Marcaccio, M.; Paradisi, M. C.; Paoluccil, F.; Balzani, V.; Denti, J. R.; Serroni, S.; Campagna, M. *Inorg. Chem.* **1993**, *32*, 3003−3009. (c) Sun, Y.; Ross, N.; Zhao, S-. B.; Huszarik, K.; Jia, W.-L.; Wang, R-. Y.; Macartney, D.; Wang, S. *J. Am. Chem. Soc.* **2007**, *129*, 7510−7511.

(27) Creutz, C. *Prog. Inorg. Chem.* **1983**, *30*, 1−73.

(28) (a) Robin, M. B.; Day, P. *Adv. Inorg. Chem. Radiochem.* **1967**, *10*, 247−422. (b) Das, A.; Scherer, T. M.; Mobin, S. M.; Kaim, W.; Lahiri, G. K. *Chem.—Eur. J.* **2012**, *18*, 11007−11018. (c) Kaim, W.; Sarkar, B.; Lahiri, G. K. *Spectroelectrochemistry*; RSC Publishing: Cambridge, U.K., 2008; pp 68−85.

(29) Lay, P. A.; Sargeson, M.; Taube, H. *Inorg. Synth.* **1986**, *24*, 291−299.

(30) Naumann, C.; Langhals, H. *Synthesis* **1990**, 279−281.

(31) (a) Sheldrick, G. M. *Acta Crystallogr., Sect. A* **2008**, *A64*, 112−122. (b) *Program for Crystal Structure Solution and Refinement*; University of Göttingen: Göttingen, Germany, 1997.

(32) Sluis, P. V. D.; Spek, A. L. *Acta Crystallogr., Sect. A* **1990**, *46*, 194−201.

(33) Lee, C.; Yang, W.; Parr, R. G. *Phys. Rev. B* **1988**, *37*, 785−789.

(34) (a) Andrae, D.; Haeussermann, U.; Dolg, M.; Stoll, H.; Preuss, H. *Theor. Chim. Acta* **1990**, *77*, 123−141. (b) Fuentealba, P.; Preuss, H.; Stoll, H.; Szentpaly, L. V. *Chem. Phys. Lett.* **1989**, *89*, 418−422.

(35) Frisch, M. J.; Trucks, G. W.; Schlegel, H. B.; Scuseria, G. E.; Robb, M. A.; Cheeseman, J. R.; Scalmani, G.; Barone, V.; Mennucci, B.; Petersson, G. A.; Nakatsuji, H.; Caricato, M.; Li, X.; Hratchian, H. P.; Izmaylov, A. F.; Bloino, J.; Zheng, G.; Sonnenberg, J. L.; Hada, M.; Ehara, M.; Toyota, K.; Fukuda, R.; Hasegawa, J.; Ishida, M.; Nakajima, T.; Honda, Y.; Kitao, O.; Nakai, H.; Vreven, T.; Montgomery, J. A., Jr.; Peralta, J. E.; Ogliaro, F.; Bearpark, M.; Heyd, J. J.; Brothers, E.; Kudin, K. N.; Staroverov, V. N.; Kobayashi, R.; Normand, J.; Raghavachari, K.; Rendell, A.; Burant, J. C.; Iyengar, S. S.; Tomasi, J.; Cossi, M.; Rega, N.; Millam, J. M.; Klene, M.; Knox, J. E.; Cross, J. B.; Bakken, V.; Adamo, C.; Jaramillo, J.; Gomperts, R.; Stratmann, R. E.; Yazyev, O.; Austin, A. J.; Cammi, R.; Pomelli, C.; Ochterski, J. W.; Martin, R. L.; Morokuma, K.; Zakrzewski, V. G.; Voth, G. A.; Salvador, P.; Dannenberg, J. J.; Dapprich, S.; Daniels, A. D.; Farkas, O.; Foresman, J. B.; Ortiz, J. V.; Cioslowski, J.; Fox, D. J. *Gaussian 09, Revision A.02*; Gaussian, Inc.: Wallingford, CT, 2009.

(36) (a) Bauernschmitt, R.; Ahlrichs, R. *Chem. Phys. Lett.* **1996**, *256*, 454−464. (b) Stratmann, R. E.; Scuseria, G. E.; Frisch, M. J. *J. Chem. Phys.* **1998**, *109*, 8218−8225. (c) Casida, M. E.; Jamorski, C.; Casida, K. C.; Salahub, D. R. *J. Chem. Phys.* **1998**, *108*, 4439−4450.

(37) (a) Barone, V.; Cossi, M. *J. Phys. Chem. A* **1998**, *102*, 1995−2001. (b) Cossi, M.; Barone, V. *J. Chem. Phys.* **2001**, *115*, 4708−4718. (c) Cossi, M.; Rega, N.; Scalmani, G.; Barone, V. *J. Comput. Chem.* **2003**, *24*, 669−681.

(38) Leonid, S. *Chemissian 1.7*; 2005−2010. Available at http://www.chemissian.com.

(39) Zhurko, D. A.; Zhurko, G. A. *ChemCraft 1.5*; Plimus: San Diego, CA. Available at http://www.chemcraftprog.com.